Citation for final published version:

Azevedo, Marco C. , Alves, Tiago M. , Fonseca, Paulo E. and Moore, Gregory F. 2018. Strike-slip deformation reflects complex partitioning of strain in the Nankai Accretionary Prism (SE Japan). Tectonophysics 723 , pp. 81-94. 10.1016/j.tecto.2017.11.023

Publishers page: http://dx.doi.org/10.1016/j.tecto.2017.11.023

Strike-slip deformation reflects complex partitioning of strain in the Nankai Accretionary Prism (SE Japan)

Marco C. Azevedo [a], Tiago M. Alves [a], Paulo E. Fonseca [b], and Gregory F. Moore [c]

[a] 3D Seismic Lab, School of Earth and Ocean Sciences, Cardiff University, Main Building, Park Place, CF10 3AT Cardiff, United Kingdom

[b] Departamento de Geologia, and Instituto Dom Luiz Faculdade de Ciências, Universidade de Lisboa, 1749-016 Lisboa, Portugal

[c] Department of Geology and Geophysics, University of Hawaii, 1680 East-West Rd., Honolulu, HI 96822, United States

ABSTRACT

Previous studies have suggested predominant extensional tectonics acting, at present, on the Nankai Accretionary Prism (NAP), and following a parallel direction to the convergence vector between the Philippine Sea and Amur Plates. However, a complex set of thrusts, pop-up structures, thrust anticlines and strike-slip faults is observed on seismic data in the outer wedge of the NAP, hinting at a complex strain distribution across SE Japan. Three-dimensional (3D) seismic data reveal three main families of faults: (1) NE-trending thrusts and back-thrusts; (2) NNW- to N-trending left-lateral strike-slip faults; and (3) WNW-trending to E-W right-lateral strike-slip faults. Such a fault pattern suggests that lateral slip, together with thrusting, are the two major styles of deformation operating in the outer wedge of the NAP. Both styles of deformation reflect a transpressional tectonic regime in which the maximum horizontal stress is geometrically close to the convergence vector. This work is relevant because it shows a progressive change from faults trending perpendicularly to the convergence vector, to a broader partitioning of strain in the form of thrusts and conjugate strike-slip faults. We suggest that similar families of faults exist within the inner wedge of the NAP, below the Kumano Basin, and control stress accumulation and strain accommodation in this latter region.

Keywords: Convergent margins; SE Japan; accretionary prism; strike-slip; transpression.

1. INTRODUCTION

The Nankai Trough is one of the most studied subduction zones in the world and delineates an active, seismogenic convergent margin under which the Philippine Sea Plate is being subducted under the Amur Plate at a variable rate of 2 to 6.5 cm/year (Miyazaki and Heki, 2001; Tsuji et al., 2014). Recent work identified a dominantly compressional area of the accretionary prism, controlled by a large "Megasplay Fault Zone" (MSFZ), on the upper continental slope of the Nankai Trough (Moore et al., 2007; Kimura et al., 2011; Moore et al., 2015). In the published literature, the MSFZ is associated with a WNW- directed (~ N120°–N125°) convergence vector that is deviated ~ 15°- 45° counter-clockwise from a direction orthogonal to the trench (e.g. DeMets et al., 2010; Tsuji et al., 2014).

Submarine accretionary prisms and associated structures are usually described by the classical critical-wedge and dynamic Coulomb-wedge theories (Davis et al., 1983; Dahlen et al., 1984), with the Nankai Accretionary Prism (NAP) being no exception (Wang and Hu, 2006). These two theories suggest a transition between a highly compressional outer wedge and a less compressional and moderately seismogenic inner wedge. As a result, Wang and Hu (2006) described the outer wedge of the NAP as comprising a series of imbricate thrust faults (i.e. reflecting a zone of low shear strength), while the inner wedge forms a zone of accreted sediment, normally acting as a backstop. The inner wedge of the NAP is characterized by the absence of active compressional structures. Reference to important strike-slip movements in the landward part of the MSFZ was made by Martin et al. (2010) and Tsuji et al. (2014), who justified these movements as reflecting a transtensional tectonic regime. Such a regime allowed the formation of small to regional-scale trench-parallel and right-lateral strike-slip faults with associated normal offsets. The same authors stated that present-day transtension is associated with oblique subduction at obliquity values as little as 15°. However, Byrne et al. (1993) also stated that a detailed picture of an underlying backstop could not be determined from surface information alone.

The theoretical interpretation of a predominantly compressional accretionary prism offshore Nankai was developed further by Byrne et al. (2009), Moore et al. (2013) and Lin et al. (2015), who confirmed the existence of a component of extension acting near the sea floor. In fact, extensional tectonics accounts for most of the modern deformation recorded in the forearc basin that overlies the inner wedge of the NAP. According to Wang and Hu (2006), Byrne et al. (2009) and Lin et al. (2015), this extensional regime is particularly active during inter- seismic cycles. Nevertheless, Lin et al. (2015) show evidence for compression at Integrated Ocean Drilling Program (IODP) Sites C0004 and C0010, seaward from the MSFZ, with a σ1 parallel to the convergence vector. Alternative interpretations consider stress decoupling between a shallow regime of normal faulting and a deeper regime of strike-slip faulting and thrusting in both the inner and outer wedges of the NAP (Moore et al., 2013; Van Tuyl et al., 2015).

Previous reference to strike-slip faults and flower structures in the outer wedge of the northeast NAP (Zenisu area) was made by Le Pichon et al. (1992; 1996). In the Nankai Trough region, flower structures and associated strike-slip faults were identified by Takahashi et al. (2002). In parallel, microseismicity studies documented the rupture of a major NW-trending, right-lateral strike-slip fault crossing the outer wedge of the NAP during the 2004 earthquake off the Kii Peninsula (M = 7.4) (Obana et al., 2005). Obana et al. (2005) proved the existence of several N- to NE-trending strike-slip fault systems operating within the Shikoku Basin. Similar strike-slip faults in the seaward part of the MSFZ, and outer wedge of NAP, have been interpreted as inherited structures from the subducted crust (Shikoku Basin) (Kodaira et al., 2006). Moore et al. (2013, 2015) focused on the Kumano Basin, which overlies the inner wedge of the NAP, to interpret two major WNW-trending strike-slip faults offsetting both the outer wedge of the NAP and the MSFZ. Notwithstanding all this work, most of recent research has been focused on the landward (Kumano Basin) and most seaward (Frontal Thrust Zone) parts of the NAP, where in-situ stresses measured at several IODP Sites have demonstrated that extension predominates at present (Lin et al., 2015).

In order to understand the structural evolution of the outer wedge of the NAP and, ultimately, of the NAP itself, it is necessary to assess: (1) where and how tectonic stresses accumulate in the prism, and (2) how shallow and deep structures relate across distinct sub-surface units. Strike-slip faulting that is not associated with the MSFZ, and within the outer wedge of the NAP, was mentioned in previous work but never fully characterized or studied, resulting in a relative under-re- presentation of this tectonic regime in the published literature. The outer wedge is considered to be the zone most actively deforming in accretionary prisms, and where the response to tectonic stresses is better expressed (MacKay et al., 1992; Park et al., 1999). Several questions remain to be addressed, some of which will have a large impact on the present understanding of NAP's tectono-stratigraphic evolution. Hence, the key aims of this work are:

1. To describe the structural framework of the outer wedge of the NAP;

2. To investigate the tectonic regime operating in the outer wedge of the NAP, as well as its related stress field(s), based on structural analyses of 3D seismic data;

3. To compare and discuss our interpretations with published information on the inner wedge of the NAP and older accretionary prisms.

2. REGIONAL GEOLOGICAL SETTING

2.1 Stress field and associated deformation styles

Knowledge on the stress state(s) at accretionary prisms is of paramount importance to assess how strain is accommodated inside them and, subsequently, to determine their deformation style(s). Taking into account that the study area is divided in an inner and outer wedge, with a transitional area that is mainly controlled by the MSFZ (Wang and Hu, 2006; Kimura et al., 2011), we follow the dynamic wedge theory of Wang and Hu

(2006) to individualize the stress states in the NAP. We use this latter theory, instead of the classic wedge concepts in Davis et al. (1983), as this latter is known to generalize the stress states for the study area.

According to Wang and Hu (2006), the mechanics of the inner and

outer wedges of the NAP are different due to the distinct behavior of their décollement, or subduction fault. In the inner part of the wedge, the décollement has a velocity weakening behavior (downdip zone) that locks it, allowing stress to accumulate until a critical point, leading to its rupture. It thus comprises a seismogenic zone. However, the inner wedge rarely ruptures compressively due to its relatively low basal friction, a character allowing for significant slip along its décollement. This means the décollement does not lock in the entire section of the NAP. In the outer wedge of the NAP (updip zone), the décollement has a velocity strengthening behavior that does allow stress to build up to a critical state, and generates a highly compressional region at the toe of the continental slope (Fig. 2A and B).

Wang and Hu (2006) argue that wedge mechanics also varies with the seismic cycle due to changes in the stress state during and after an earthquake. During an earthquake, $\sigma1$ is subhorizontal and the décollement slips, pressurizing the outer wedge into elastic or permanent compressive deformation. In contrast, the inner wedge is in a stable extensional state, as shear stress is null due to slip in the décollement. After an earthquake, the outer wedge records interseismic relaxation that is accompanied by a decrease in shear stress, seaward movement of this part of the NAP, and an increase in the dip of $\sigma1$, whereas the inner wedge starts to become more compressional as shear stresses start to build up again.

Several methods have been applied to IODP data to define the stress field and deformation style(s) currently operating across the NAP, and on the incoming Philippine Sea Plate (Shikoku Basin) (Wu et al., 2013; Lin et al., 2015; Huffman and Saffer, 2016; Chang and Song, 2016). These papers not only show important changes in the stress field and deformation style(s) across the NAP, and between the NAP and Shikoku Basin; they also show results that are not consistent for the same IODP sites. This is due to the fact that different methods have been applied to define these stress field(s) and associated deformation regime(s), and that measurements were taken at different depths and scales of observation.

Wu et al. (2013) used a compilation of Formation Micro Imager (FMI), Logging While Drilling (LWD) and core data to calculate the magnitudes of maximum (σ_{Hmax}) and minimum (σ_{hmin}) horizontal stresses. The magnitudes were constrained in stress polygons to derive the field stress in different areas of the NAP and Shikoku Basin. At IODP Site C0009, in the inner wedge of the NAP and at ~1540 metres below sea floor (mbsf), Wu et al. (2013) showed that σ_{Hmax} and σ_{hmin} correspond to σ_1 (maximum stress) and σ_3 (minimum stress), respectively. Here, σ1 is perpendicular to the trench direction (which is NE-trending), and the deformation style is strike-slip faulting. However at IODP Site C0002, in the seaward part of the inner wedge (at ~ 1000 mbsf), the same authors estimated a NE-trending σ_{Hmax} where $\sigma_v > \sigma_{Hmax}$, a configuration that reflects a normal faulting regime. At IODP Site C0006, in the Frontal Thrust Zone (~476 mbsf), Wu et al. (2013) interpreted a normal faulting regime with a vertical σ_1 (σ_v), but close to strike-slip faulting due to σ_{Hmax} being NW-trending and only 0.5 MPa lower than σ_v. In the Shikoku Basin, at IODP Site C0011 (~610 mbsf), the stress field and deformation styles are similar to IODP Site C0002, but again very close to strike-slip faulting due to the minor difference in magnitude between σ_v and σ_{Hmax}. Despite these results, Wu et al. (2013) state that their stress analysis was limited by the total drilling depth, borehole conditions and deviations in the slip deficit method, thus returning less reliable results at relevant depths.

Lin et al. (2015) used a similar approach to Wu et al. (2013) in a larger number of IODP Sites across the NAP and Shikoku Basin, together with hydraulic fracturing experiments and anelastic strain recovery (ASR) measurements on retrieved cores. This approach allowed a detailed investigation of stress states across the NAP and Shikoku Basin, in three dimensions, leading to the conclusion that, overall, the NAP is currently undergoing a (inter-seismic) extensional regime.

According to Lin et al. (2015), the sediment cover overlying the inner wedge of the NAP (Kumano Basin) has a vertical σ_1 and expresses a normal faulting regime. However, the strikes of σ_{Hmax} at IODP Sites C0009 and C0002 agree with the results in Wu et al. (2013). The transition from the Kumano Basin strata to the inner wedge of the NAP is accompanied by a change in σ_1 from vertical to sub-horizontal, where $\sigma_{Hmax} = \sigma_1$, and by a change from normal to strike-slip and thrust faulting. At the MSFZ, IODP Site C0001 shows a similar stress distribution (and deformation style) to that of IODP Site C0009 with depth, with the change occurring at ~500 mbsf. However, at IODP Sites C0004 and C0010, where the hanging-wall of the MSFZ was drilled, σ_1 is interpreted to be sub-horizontal and parallel to the plate convergence vector, reflecting thrust and strike-slip faulting regimes. In the shallower part of the hanging-wall of the Frontal Thrust Zone, drilled at IODP Sites C0006 and C0007, Lin et al. (2015) interpreted a similar stress field and deformation style to the shallow part of IODP Site C0001. Finally, in the Shikoku Basin, the interpretation of IODP Site C0011 coincides with the results in Wu et al. (2013), while at IODP Site C0012 ASR analyses show evidence for strike-slip and reverse faulting with a NE-trending σ_{Hmax}. In such a setting, Lin et al. (2015) state that, at present, the overall NAP is dominated by a shallow ex- tensional regime and a relatively deep strike-slip to reverse faulting regime, mainly due to stress field reorganization in the areas where σ1 becomes σ_{Hmax}. This transition between different tectonic regimes at depth is often referred to as Extension-Compression Depth (ECD) and there is consistent data suggesting that the ECD is highly variable along the entire NAP, in both the inner and outer wedges, depending on the thickness of the overlying sediment cover (Lewis et al., 2013; Van Tuyl et al., 2015; Lin et al., 2015). Lin et al. (2015) refer that principal stresses permute in the deeper levels of the NAP, but that sediment cores have yet to be recovered at such depths.

Recently, Chang and Song (2016) integrated borehole breakouts, drilling-induced tensile fractures and leak-off tests at IODP Site C0002 to interpret tectonic stresses (up to a depth of ~2000 mbsf) at the seaward limit of the inner wedge of the NAP. They concluded that deformation in this latter region varies between strike-slip and normal faulting as a result of σ_{Hmax} and σ_v having similar magnitudes. They stress that σ_{Hmax} is NE-trending above the MSFZ. The same authors postulate that strike-slip and extensional structures are found in both core and regional seismic data.

In the Muroto Transect, outside our study area but still in the NAP, Huffman and Saffer (2016) showed similar results and interpretations to the authors previously mentioned. Stress states at the toe of NAP are likely associated with strike-slip or thrust faults across the active Frontal Thrust Zone down to a depth of ~800 mbsf. The uppermost 300 mbsf are near thrust failure, where $\sigma_{Hmax} > \sigma_v$. However, Huffman and Saffer (2016) conclude that the stress state in the upper 300 mbsf changes into a normal faulting regime at depth, where $\sigma_v > \sigma_{Hmax}$. These authors recognize the large uncertainties associated with the parameters used in their stress analysis.

It is important to highlight that limitations such as the depth and location of the boreholes, and conditions in which data were acquired, can influence the analysis of regional stress states. Nevertheless, there seems to be an overall consensus that the NAP is a compressional structure currently dominated by shallow normal (Wu et al., 2013; Lin et al., 2015; Chang and Song, 2016) and strike-slip (Huffman and Saffer, 2016; Chang and Song, 2016) faulting regimes. Borehole data are clear that shallower stress conditions differ from those affecting deeper strata, but the lack of deep measurements does not allow definite conclusions about the stress field and deformation styles operating at depth, and on the relationship between the shallow and deep settings of the NAP. Furthermore, it is clear that strike-slip is an important deformation style within the NAP that is yet to be characterized in detail.

Against this backdrop, three-dimensional interpretations of stress magnitudes and tensors along the NAP are not unequivocal at some drilling sites. Furthermore, stress field studies have not been performed in the outer wedge of the NAP due to the lack of borehole data in this region, and at higher depths within the inner wedge (below the sediment cover of the Kumano Basin). This means that extrapolations based on few localized wells in the MSFZ and inner wedge are not fully reliable, and a detailed analysis of 3D pre-stack depth migration (PSDM) seismic data from the outer wedge of the NAP can be crucial to understand its structural and stress evolutions.

2.2 Seismic stratigraphy

Most lithological information acquired in the NAP derives from core and well-log data gathered by the NanTroSeize Project. IODP Sites C0018A (Figs. 1, 2B and C) and C0006 (Fig. 1A), which are respectively located seaward of the MSFZ (in the outer wedge of the NAP) and in the Frontal Thrust Zone, provide valuable lithological and stratigraphic information on the shallow sedimentary cover, uppermost part of the accretionary prism, and underthrusted sediments from the Philippine Sea Plate. Multiple IODP campaigns reached strata within the outer wedge of the NAP, and collected stratigraphic evidence to show that the study area is mainly composed of a relatively thin Unit I (Expedition 315 Scientists, 2009; Expedition 316 Scientists, 2009; Kimura et al., 2011; Strasser et al., 2014). Slope sediments were accumulated above an angular unconformity separating them from an underlying Unit II, this latter comprising strata belonging to the upper part of the accretionary prism (Kimura et al., 2011) (Fig. 2D). In addition, cores collected at IODP Site C0006 drilled through a deep Unit III composed of underthrusted deep-marine sediment from the subducting Shikoku Basin.

Unit I can be up to 2.4 Ma old and comprises slope-apron fine- grained turbidite facies spanning the latest Pliocene-Holocene. Data from IODP Sites C0008 and C0018A (Expedition 315 Scientists, 2009; Expedition 316 Scientists, 2009; Expedition 333 Scientists, 2012) di- vided Unit I into Units Ia, Ib and Ic, which mark a gradual transition from upper-slope apron facies to base of slope apron facies. Unit Ia comprises hemipelagic mud and silty-clay sequences intercalated with multiple ash layers. Unit Ib is composed of hemipelagic mud, silty clay and silty turbidites with ash layers. Finally, Unit Ic reflects sediment deposited above Unit II and it is characterized by turbiditic sand and sandy silt intercalated with mud and ash layers (Expedition 315 Scientists, 2009; Kimura et al., 2011; Alves et al., 2013; Strasser et al., 2014).

IODP Sites C0006, C0008 and C0018 (Expedition 315 Scientists, 2009; Expedition 316 Scientists, 2009) define Unit II as reflecting the uppermost part of the accretionary prism. This unit is considered to be Pliocene in age or older (Expedition 315 Scientists, 2009; Expedition 316 Scientists, 2009; Alves et al., 2013). It comprises accreted sediments with mudstone- to sand-dominated lithologies (Expedition 315 Scientists, 2009; Kimura et al., 2011; Alves et al., 2013; Strasser et al., 2014).

Unit III was identified below Unit II in the Frontal Thrust Zone, at IODP Sites C0006 and C0007 (Expedition 316 Scientists, 2009), and comprises hemipelagic mud interbedded with volcanic ash and tuffs. Unit III is deformed by thrust faults and transitions at depth into Unit IV, which represents underthrusted Shikoku Basin sediment (Expedition 316 Scientists, 2009).

In the inner wedge of the NAP, the presence of an overlying forearc basin (Kumano Basin), and underlying thrust-and-fold accretionary prism, agrees with the stratigraphic units defined by IODP Expeditions 315 and 316. However, slope sediments are relatively thin and dis- continuous in the outer wedge of the NAP, having been removed by erosion at places (Van Tuyl et al., 2015). This means that Unit I may not exist in most of the outer wedge. Furthermore, it is difficult to characterize the strata inside the outer wedge of the NAP due to the lack of borehole data crossing the complex, folded sequences that form this same prism. In the study area, 3D seismic data show that the accretionary prism should be divided in several tectono-stratigraphic units instead of being classified as Unit II and Unit III (Fig. 2B).

As the focus of this work is the structural interpretation of the outer wedge of the NAP, we used published information on Unit I (due to the extensive core/log data acquired in this latter) to propose an adaptation of the tectono-stratigraphic division of the outer wedge of the NAP in Park et al. (2010). In our work, the upper part of Unit A comprises the overthrusting package that includes Unit II. Unit B is the Low Velocity Zone

(LVZ) identified by Park et al. (2010) and Kamei et al. (2012). Unit C is the underthrusting part of the accretionary prism (Figs. 2A and B). The deepest unit in the study area corresponds to subducted oceanic crust in which seismic resolution is significantly lower. Based on Park et al. (2010), Unit C represents underthrusted sediments that under- plate Unit A as defined in this work, while maintaining a critical taper in the modern accretionary prism. This geometry allows the seaward growth of Unit A to produce the LVZ and associated Unit B. In contrast, Kamei et al. (2012) propose a thicker LVZ that includes both Units B and C from Park et al. (2010), with a décollement on top of Unit C.

The seismic data used in this work show clear evidence for two units of low reflectivity separated by a strong seismic reflection (décollement), strengthening the idea that Units B and C represent similar lithologies, i.e. Unit B originating from the underthrusting or underplating of Unit C (Bangs et al., 2009; Park et al., 2010; Kamei et al., 2012). Bangs et al. (2009) discussed the possibility of the décollement being initially at the top of the LZV (Unit B), changing later to its present-day position. Such a character suggests a similar lithology across Units B and C, but with both units reflecting distinct tectonic and rheological behaviors.

3. STUDY AREA AND METHODOLOGY

The study area is located in the southeast coast of Japan, just off the Kii Peninsula, within what is known as the Kumano Transect (Fig. 1A). In this transect, a 3D pre-stack depth migrated (PSDM) seismic volume was acquired across the Nankai continental slope as part of the Nankai Trough Seismogenic Zone Experiment (NanTroSEIZE) (Figs. 1B and 1C). The study area comprises the southern half of the acquired 3D PSDM seismic block, imaging the Imbricate Thrust and Frontal Thrust Zones just seaward of the MSFZ (Moore et al., 2001; Park et al., 2002; Tobin and Kinoshita, 2006) (Fig. 1B-C). This region is also known as the outer wedge of the NAP.

Mapping and interpretation of seismic horizons, complemented by the compilation of attribute maps, form the basis of our structural analysis (Figs. 2 and 3). The interpreted seismic volume has an inline spacing of 12.5 m, a crossline spacing of 18.75 m, and was acquired using a 2-source array with four receiver cables at a distance of 150 m. Each receiver cable was 4500 m long, with 360 receiver groups spaced 12.5 m, and was able to acquire nominal 60-fold data. Data processing included pre-stack multiple removal and data conditioning (e.g., amplitude recovery, time-variant filtering, and predictive deconvolution) followed by 3D pre-stack depth migration (Moore et al., 2009). Seismic resolution can reach < 5 m at the depth of the shallower faults in this paper, for a range of 6–10 m in the deeper strata based on the dominant wavelength of ~24 m observed on synthetic logs and seismic profiles. The main limitation of this method results from the fact that it is only possible to observe, map and interpret structures that are within this latter range in seismic resolution.

According to Roberts (2001) and Chopra and Marfurt (2005, 2007a, 2007b), attribute data such as coherence and curvature have crucial importance to the 3D interpretation of seismic data. Both attributes are particularly helpful in structural analyses, as they enhance faults that are often not recognized on vertical seismic profiles or time-structure maps alone. Volumetric curvature is a property that measures lateral changes in dip-magnitude and dip-azimuth waveforms (Mai et al., 2009). The presence of fractures and small faults is closely related to reflection curvature. In this work, maximum curvature is used to visualize small-scale faults and later obtain measurements of maximum horizontal displacements from them. In addition, coherence comprises a technique cross-correlating seismic amplitudes in adjacent traces, and has a proven record of efficiently portraying faults by measuring lateral changes in waveform (Chopra and Marfurt, 2005; Mai et al., 2009). These attributes are automatically extracted from specialized seismic interpretation software, such as Schlumberger's Petrel® used in this work, but it is necessary to choose a horizontal time- or depth-slice that is deep enough to intersect a wide range of well-resolved structures. After careful interpretation of the 3D PSDM seismic volume, we selected an area that had been significantly affected by thrust-and-fold structures at a depth of 3840 m.

In this work, we classify the interpreted faults based on their strikes as there is a direct relationship between their geometry and the observed deformation styles in the outer wedge of the NAP. Strike measurements are automatically undertaken by the seismic interpretation software after faults are mapped. For curved faults and fractures one measurement is taken as the average strike, which coincides with the best fitting straight line to the curve. Taking into consideration that several authors agree with the interpretation of distinct deformation regimes at shallow and deep levels of the NAP (e.g. Lin et al., 2015; Van Tuyl et al., 2015; Chang and Song, 2016), a classification based on the length of imaged faults, and their depth, can also be used. However, such a classification will bear no relation to either the geometry or the deformation styles of such structures, as the boundary between shallow and deep structures occurs at a variable depth.

Van Tuyl et al. (2015) explain that the depth of the ECD surface on 3D seismic data is markedly variable, being shallower in the outer wedge than in the inner wedge, and clearly related to the thickness of overlying slope sediment (Unit I). Therefore, in order to classify the different families of faults in terms of length and depth they reached, we consider shallow structures as affecting the uppermost part of the NAP (Units A and B), and deep structures as those propagating from the décollement, intersecting the décollement, or offseting Unit C and oceanic crust.

Seismic attribute mapping provides the basis for statistical analyses of geometry, kinematics and dynamics of the main faults in this work (Fig. 3). The strikes of thrusts and conjugate sets of strike-slip faults were measured prior to the estimate of stress and paleostress fields from dihedral angles (Hancock, 1985). This latter estimate provided the basis for our structural analysis, allowing the 3D mapping of small- and large-scale faults and fractures, and detailed descriptions of their geometry, kinematics and dynamics. Our approach included the quantitative characterization of faults' strike and their throws and horizontal (strike-slip) displacements, together with quatitative analyses of fault dips.

4. STRUCTURAL ANALYSIS

The Imbricate Thrust and Frontal Thrust Zones chiefly comprise NE- striking thrusts formed by horizontal shortening, dipping to the NW (in- sequence) or SE (out-of-sequence and back-thrusts) (see Moore et al., 2001; Gulick et al., 2004; Strasser et al., 2011). Nevertheless, seismic attribute maps reveal the existence of at least two more families of faults with conjugate geometries; a first trending WNW to E-W and a second trending N to NNW (Fig. 3). Two major NW-trending faults, belonging to the first of the two fault families have already been mapped and described by Moore et al. (2013) as displacing surface ridges within the Imbricate Thrust Zone.

4.1 NE-trending faults (shallow-deep)

Main structures within the NAP comprise curved NE-trending (azimuth: 40° to 60°) thrusts and back-thrusts dipping toward the NW and SE (Moore et al., 2001) (Figs. 2A–B, 3A–C, 4A and 4C). Thrust faults are clearly associated with the formation of SE-verging anticlines with bathymetric expression on the sea floor (Figs. 1, 2A–B, 3 and 4). Kinematic indicators in these thrusts reveal a secondary right-lateral component in the form of: (1) an increase in the number of back-thrusts in the larger anticlines toward NE, a character denoting accumulation of strain in this same direction; (2) possible horse-tail splay terminations of thrusts occurring at their NE tips (Fig. 3A–B); and (3) slight vergence of hanging-wall anticlines toward the NE (Fig. 4C). Note that kinematic indicators are not observed in all thrusts.

Most of the shallow and shorter NE-trending thrusts are clearly primary structures, as they are intersected by or offset other faults with different trends (Fig. 4A). Yet, the deep and large-scale thrusts do not seem to be affected by the same structures (Fig. 4A and C). Whether the deep thrusts are older structures displaced by younger faults with different trends, or these younger faults propagate from deeper thrusts, is a point under discussion as we cannot ascertain clear cross-cutting relationships among all interpreted structures. Either way, the observed geometries suggest that faults are diachronous; the larger, deeper thrusts moved before and after the time of formation of the remaining faults with different trends.

The deep thrust faults root in (or start from) the décollement, usually at a depth between 6.5 and 8 km, only intersecting it in the frontal part of the NAP (Fig. 2A–B). In addition, the deep thrusts usually show synthetic (but shallow) thrust faults and antithetic back-thrusts (Fig. 2A–B, 4A and 4C).

4.2 WNW- to E-W-trending faults (shallow-deep)

One of the most striking features in the NAP is the steeply dipping WNW-trending F1 fault (azimuth: 110° - 115°), a structure ~8 km long and ~3km high, at places intersecting the basal décollement and subduction channel (Fig. 1, 3A–C and 4B–C). The geometry and dip direction of F1 are not constant, suggesting linkage of WNW-trending faults during its formation. Fault F1 displaces the majority of thrust anticlines imaged on seismic data and exhibits a right-lateral strike-slip movement in map view (Fig. 1 and 3A–C). In contrast, vertical seismic profiles reveal normal throws for this same fault (Figs. 4B–C). Its NW tip shows multiple faults with similar trends and slip directions (Fig. 3A–C and 4B). It is not possible to define if these minor faults are branching out of a deeper fault, or if they reflect a highly deformed zone near the sea floor as revealed by the presence of several minor faults (Fig. 4B). Nevertheless, the SE tip of F1 splays out in several branching faults that join or stop against other thrusts (Fig. 3A–C). Similar fault geometries to F1 have been described as negative flower structures in which the horizontal component is dominant (Harding, 1985).

The F1 fault separates two distinct structural domains: (1) a domain to the N where left-lateral slip predominates, and (2) a domain to the S where right-lateral motion is significant (Fig. 3C). At a smaller scale, there are structures with similar kinematics to F1, trending WNW-ESE to E-W (azimuth: 85°–115°), with variable lengths (Fig. 3A–C). These structures comprise a range of pure strike-slip to oblique-slip faults. Their normal slip component (Figs. 3 and 4) can result from normal (dip-slip) movement or comprise an apparent displacement associated with strike-slip motion. The variable throw values recorded, usually increasing toward the surface, together with contrasts between total offset and its bathymetric expression (Fig. 3D), indicate that the observed normal slip can be an apparent slip from right-lateral faults intersecting an inherited fold-and-thrust structure dipping to the NW (Fig. 4C). Furthermore, trend-parallel horizontal offsets are much larger than fault throws, up to a factor of 2 to 3 (Fig. 3C–D). It is important to highlight that not all WNW to E-W structures show lateral movement, suggesting that strike-slip motion is recent or periodically alternates in response to the reactivation of deep structures in the NAP.

Despite F1 being a deep structure that reaches, and seemingly intersects, the décollement, not all WNW to E-W faults propagate beyond a depth of 1 km below the sea floor. However, when compared with other strike-slip faults, WNW to E-W faults are much deeper. Similar fault patterns have been found on other convergent margins, but at larger scales of observation (Lewis et al., 1988; Platt et al., 1988).

4.3 NNW- to N-trending faults (predominantly shallow)

In the outer wedge of the NAP there are several NNW- and N- trending structures (azimuth: 345°–10°) dipping toward the W or sub- vertical, rarely reaching the sea floor (Fig. 3A–C and 4). These faults normally exhibit a left-lateral strike-slip motion, and a variable normal throw (Fig. 3C). Faults trending N to NNW show variable lengths but usually occur in thrust anticlines, rarely extending into their adjacent synclines. Their vertical extension is variable, from a few meters to hundreds of meters, seldom affecting the sea floor. In some cases, similar structures are observed on both the hanging-wall and footwall of major thrust faults, intersecting some of the deeper thrusts in the NAP (Fig. 4A and C).

4.4 Normal faults

Minor normal faults on the scale of tens of meters have been observed and are normally confined to the uppermost part of the sediment cover, as previously described by Strasser et al. (2011) and Van Tuyl et al. (2015). These minor faults tend to follow the trends of strike-slip faults, but seldom those of thrust faults (Fig. 5). The normal faults following the trend of strike-slip faults have been classified as normal as they show minor throws without any evidence for horizontal movement. However, they can comprise oblique-slip faults in which their horizontal displacement is below the horizontal seismic resolution of the 3D PSDM volume.

4.5 Deep structures

Some of the structures previously identified by Tsuji et al. (2013) as affecting the décollement or units below were also mapped in this work. These deep structures normally show a larger complexity in their geometry and kinematics (Figs. 2B, 6 and 7). According to Tsuji et al. (2013), some of the deep faults imaged on seismic data are inherited structures from Philippine Sea Plate's oceanic crust. These inherited structures do not only control the thickness of the accretionary prism, but also its structural framework. These structures include active intra- oceanic thrusts (Fig. 2B) and some strike-slip faults resulting from lateral movement at the edges of the thicker parts of the NAP. In the outer wedge of the NAP, these intra-oceanic thrusts will control the location of main thrust faults within the Imbricate Thrust Zone. How- ever, in this work we identified several deep-rooted faults with similar directions to the previously described strike-slip faults.

Despite their larger structural complexity, deep structures show similar trends to features observed in the NAP, especially when referring to strike-slip fault families (Fig. 6). It is equally important to highlight that these deep structures reach depths larger than 6 km below the sea floor, rooting at and displacing the décollement and underlying units. Some of these structures show relative displacements that do not laterally or vertically agree with a pure extensional or compressional regime of deformation (Fig. 6). Thus, only a strike-slip or a combined regime of deformation can justify such a displacement pattern. This combined regime often generates distributed deformation zones in which strike-slip motions may not be the same as the regional strike-slip movement (McKenzie and Jackson, 1986). In addition, branching and splaying of deep structures are observed and increase upward, resulting in a continuous decrease in the displacement of these splays/branches and, consequently, in a shallower chaotic zone of fracturing that rarely offsets the sea floor (Fig. 6). The fact that these branched faults (and fault F1) reach the sea floor, suggests they may be active or were recently active.

As previously discussed, fault F1 is a deep fault that roots in the décollement or in deeper strata. However, the near-seafloor extension of this fault seems to vary along strike (compare Fig. 4C and Fig. 6). In Fig. 4C, which is located a few kilometers NW from Fig. 6, we observe a sharp fault F1 cutting through the outer wedge of the NAP, reaching the sea floor without any major branching or splaying (see also Fig. 6). This geometry can be related to differential movement of different sets of the minor faults that compose fault F1, or to the geometrical interaction between this and other faults, such as fault F2 (Fig. 3).

Significant displacement is observed in Unit C in other areas of the outer wedge of NAP, in addition to the area shown in Fig. 6, and con- firms a positive correlation between deformation in the décollement and underlying units, and deformation in Unit A (Fig. 7). Thus when the oceanic crust, Unit C and, consequently, the décollement are folded and fractured, Unit A usually presents a much greater deformation and structural complexity (see Tsuji et al., 2013).

In Fig. 7B two faults follow the same strike (and are in the same position) of strike-slip fault F1, displacing Unit B and branching upward into a chaotic deformation zone within the entire overlying Unit A. These deep structures have a throw of 500–1000 m, which is significantly larger than the throws of any other thrust in the outer wedge of the NAP, and larger than the horizontal displacement of F1 (ca. 600 m). These thrust faults were previously interpreted as a single major intra-oceanic thrust (Tsuji et al., 2009; Tsuji et al., 2013). Once more, it is possible to observe an upward decrease in their throws, probably occurring in association with splaying/branching towards shallower strata. The observed geometry suggests a variation from a deep regime where dip-slip displacement is larger than horizontal dis- placement, to a shallow regime where dip-slip displacement is smaller than horizontal displacement.

5. DISCUSSION

5.1 Significance of strike-slip faulting in the outer wedge of NAP

Despite clear evidence for primary compressional deformation across the NAP (Moore et al., 2007; Kimura et al., 2007; Kimura et al., 2011), the analysis in this paper reveals that strain in this region is also accommodated by secondary strike-slip deformation. This observation has a significant impact in the structural framework of the NAP and the way(s) stress release and accumulation occur in the region. Therefore, the outer wedge of the NAP is being affected by two main families of strike-slip faults; WNW-trending to E-W right-lateral faults, and NNW- to N-trending left-lateral faults. Their spatial distribution is controlled by F1, which divides two different structural domains. The fact that: (1) the horizontal displacement (120–600 m) is two or three times larger than dip-slip displacement (< 40 m), (2) fault throws are variable in both its magnitude and nature of movement, and (3) normal slip in faults does not have the same expression on the sea floor, lead us to consider these structures to be strike-slip faults (Fig. 3). We interpret that most of the normal slip observed is an apparent slip developed in a fold-and-thrust sequence dipping to the NW, itself affected by strike-slip faulting with significant lateral motion (Fig. 4). Lateral movement is particularly noted on structural maps, where the WNW- to E-W trending and the NNW- to N-trending strike-slip faults are conjugate (Fig. 3).

Fig. 4B exhibits a likely negative flower structure with an associated normal-slip component suggesting that, within a dominant transpressional regime, there could be local zones in which transtension is favored in a distributed deformation pattern (McKenzie and Jackson, 1986). This ‘flower structure’ can also result from the combined effect of strike-slip and thrust movements as: (1) the structural domain to the N of F1 exhibits larger horizontal shortening and tilting than the S domain (Fig. 8), and (2) the curved shape of the NW tip of F1 exhibits a larger throw and horizontal slip as its angle approaches a direction perpendicular to the trench. This is the first mention of flower structures in the Imbricate Thrust and Frontal Thrust Zones of the NAP, although other flower structures have been identified in parts of the Nankai Trough and associated with a lateral component of motion (Le Pichon et al., 1996; Takahashi et al., 2002).

There are several structures that follow the same orientation as these conjugate strike-slip faults, but without revealing lateral slip. These structures are relatively shallow and exhibit small normal slips to no dip-slip displacement (Figs. 4C and 5). Also, they do not have any bathymetric expression. These latter structures can result from one of two scenarios: (1) blocks bordered by well-developed strike-slip faults experienced some torsion/rotation that is accommodated by extension, (2) accommodation of lateral movement in blocks bordered by strike- slip faults is no longer possible, or is significantly hindered, with new strike-slip or oblique-slip faults being formed as a result.

The observation that deep structures affecting the décollement and underlying units follow the direction of shallow structures (Figs. 1, 6 and 7), highlights the fact that the uppermost strata in the outer wedge of the NAP (Unit A) is influenced by deeper faults. Some of these latter faults have been identified as inherited structures from the subducted Philippine Sea Plate (Tsuji et al., 2013). The fact that some strike-slip faults branch upward, affecting the sea floor, indicates that the outer wedge is slipping during inter-seismic periods and strain is accommodated as transpressional deformation. Fig. 1 shows that some of the thrusts offsetting Unit C and the décollement may not be related to an inherited structure from the Philippines Sea Plate. Considering that some of these thrust faults reach the sea floor, affecting the local bathymetry, they may not be entirely associated with tectonic activity along the MSFZ but, instead, with faulting in Unit C and overlying décollement.

The interpreted seismic volume points to a compressional accretionary prism where synthetic and antithetic thrusts and strike-slip faults are the major structures responsible for deformation in the outer wedge of the NAP, and provides scant evidence for extensional de- formation. However, a dominant strike-slip or compressional de- formation can be responsible for the formation of near-seafloor extensional structures due to gravitational collapse or through the accommodation of deformation at shallower levels of the NAP (Fig. 5), as recorded in other compressional settings (Shelton, 1984; Burchfiel and Royden, 1985). Therefore, we corroborate the presence of a variable ECD within the NAP that is strictly associated with the thickness of the sediment cover (Van Tuyl et al., 2015). In the NAP, the dominant deformation style is not extensional and the shallower extensional regime is a consequence of a dominant transpressional regime.

5.2 Estimates of maximum horizontal stress

Thrust and strike-slip faults identified on seismic attribute maps had their strikes measured for statistical purposes, and to identify the range of strikes for each fault family (Fig. 3). The measured range of strikes was simplified to a mean azimuth so we could apply a dihedral angle method (Hancock, 1985) to interpret the maximum horizontal stress or paleostress responsible for the structures described in this paper. We recognize this latter method as simplistic, but still comprising a valid approach for determining the principal stresses at the time of failure. According to Hancock (1985), an extension fracture is initiated perpendicularly to σ3 in the principal stress plane containing σ1 and σ2, and conjugate hybrid or shear fractures enclose an acute bisector parallel to σ1 (Hancock, 1985). When applying this method, we used two-dimensional strike data from attribute seismic maps and, as a result, we only estimate the maximum horizontal stress.

The mean azimuth of the NE-trending thrusts and back-thrusts is 50°. If we were to consider a pure compressional regime for the formation of the NAP, we would infer a maximum horizontal stress trending perpendicularly to this fault family, i.e. 130°. However, as previously discussed in this work, the NAP accretionary prism is characterized by a dominant strike-slip fault regime arranged in a conjugate geometry, where one of the families (NNW- and N-trending) has a mean azimuth of ~357.5° and the other (WNW-ESE to E-W trending) has as a mean azimuth of ~100°. The calculated bihedral/bisector (θ) angle of this conjugate system is ~38.75°, a value that is larger than the 30° generally defined by the Anderson's Theory (Anderson, 1905). How- ever, Anderson (1905) and Hancock (1985) postulate that in natural conditions θ should be < 40°–45°, depending on the confining pressure

and resistance to failure of deformed strata, as the value θ = 30° was calculated in laboratorial conditions for isotropic and mainly non-natural material. The existence of an abnormal pore-fluid pressure within the NAP (Tsuji et al., 2008; Kodaira et al., 2004) justifies the larger dihedral angle calculated here, as it normally increases proportionally to the confining compressive pressure (Ramsey and Chester, 2004). Ismat (2015) defends that the dihedral angle can also increase within the hinge regions of folds, which is one of the main structural features of the NAP.

The bihedral angle of ~38.75° calculated in this work places the maximum horizontal stress at an average azimuth of 138.75°. This is not far from the mean azimuth of 130° inferred from thrust and back- thrust faults in the study area, thus representing a difference of 8.75°. It also represents a difference of < 20° from the general convergence vector of azimuth 120°–125° defined by DeMets et al. (2010). However, Tsuji et al. (2014) state that the convergence vector can deviate up to 30° from the orthogonal direction to the trench, meaning that the calculated mean azimuth for the maximum horizontal stress can also be influenced by this angular relationship.

The minor difference between the azimuths inferred from NE- trending thrusts, and the strike-slip conjugate system, can be related to: (1) a minor rotation of the stress field due to either progressive de- formation or alternating seismic and inter-seismic periods, as suggested by Wang and Hu (2006), or (2) related to the existence of a pre-existing NE-trending structures in the anticlines and (deep) structures inherited from the subducting Philippines Sea Plate (Tsuji et al., 2013). In this latter case, deep structures may have controlled the strain accommodation and stress response within the NAP, particularly when strike- slip becomes the favored regime of deformation.

It was not possible to calculate the exact azimuth of the convergence vector in the study area, but our analysis still provides a mean azimuth for the maximum horizontal stress. Despite the high probability of a σ_{Hmax} parallel to the convergence vector between the Amur and the Philippine Sea Plates, we must assume they do not match. We must also assume that any mismatches between the calculated azimuth for maximum horizontal stress, and the azimuth for the convergence vector, may be due to structural complexity in the NAP or angular errors associated with our geometric analysis - which was purely based on the interpretation of 3D seismic data. Structural complexity is related to the diffuse accommodation of strain in the outer wedge of the NAP, caused by the presence of inherited deep structures (Tsuji et al., 2013) that control the deformation in the upper part of the outer wedge, even with a main convergence vector of azimuth 120°-125°.

We recognize that our estimations for the stress state in the outer wedge of the NAP represent a past average stress state. However, the fact that some of the strike-slip faults offset the sea floor, and that strike-slip and thrust faults mutually intersect and offset each other, suggests that this stress state may still be active. Such a postulate implies that the outer wedge is not experiencing a period of coseismic relaxation and, instead, is being compressed by possible aseismic slip of subduction faults (Wang and Hu, 2006).

5.3 Deformation styles in the outer wedge of the NAP and comparison with other accretionary prisms

In the Kumano Basin, Moore et al. (2013) identified four populations of normal faults in strata overlying the NAP. They share similar trends to faults interpreted in this paper (Figs. 9A–B). Phase 1 normal faults correspond to our NE-trending thrust and back-thrust faults, whereas phase 2 and phase 3 normal fault populations respectively match the orientation of NNW- to N-trending left-lateral strike-slip faults and WNW-trending to E-W right-lateral strike-slip faults. This character suggests that normal faults generated in the sediment cover of the NAP, and in Kumano Basin sediment, can be the near-surface expression of gravitational collapse or local adjustments from structures active at deep levels, imposing anisotropic conditions in both the inner and outer wedges of the NAP. Similar syn-sedimentary normal faults have been described for the Makran accretionary prism as responding to prism overthickening caused by underplating (Platt et al., 1988).

According to Boston et al. (2016), the inner wedge of the NAP inherited a pre-existing structural framework that is chiefly composed of thrusts similar to those interpreted in the outer wedge. Compression remains the main deformation style operating in the NAP. The structural data collected by Boston et al. (2016) in the inner wedge also agree with the trends of structures and fault families in this work; the majority of the structural data in Boston et al. (2016) correlate with our synthetic thrust faults. The few deep structures identified by Boston et al. (2016) are geometrically related to our strike-slip families (Fig. 9A and C). However, no reference to strike-slip is made in their work.

Taking into consideration Moore et al. (2013) and Boston et al. (2016) interpretations, structures within the inner wedge and the Kumano Basin are geometrically similar to structures identified and mapped in this work, and variations in strikes and faulting regimes can be entirely related to strain partitioning from the Frontal Thrust Zone to the inner wedge or related to the MSFZ. This interpretation suggests that structures across the NAP somewhat reflect the same tectonic setting, but result in different structural expressions depending on the local geological and physical conditions. In the outer wedge, there is no evidence for a dominant extensional deformational style, especially when considering that all normal faults are small and follow the same trend of deeper strike-slip (and thrust) faults. Instead, evidence points toward the co-existence of both compressional and strike-slip styles of deformation.

Cross-cutting relationships between strike-slip faults and thrusts are not always easy to observe due to the NAP's structural complexity and poorer seismic resolution at depth. However, structural data in this work suggests a primary fold-and-thrust framework that is later intersected by relatively recent thrust and strike-slip structures. The chronology between these latter strike-slip and thrust faults is not conclusive as they seem to have been reactivated simultaneously: 1) as a con- sequence of a transpressional regime, where both thrusting and strike- slip faulting coexist, or 2) due to alternations between co-seismic and inter-seismic periods favouring the generation of thrusts and strike-slip structures in discrete tectonic pulses.

We favor the first hypothesis above due to the fact that a transpressional regime, in which both thrusting and strike-slip can develop, corroborates the information discussed in Section 5.2. Furthermore, the chronological order proposed by Moore et al. (2013) for the normal fault populations in the Kumano Basin matches the postulate of an initial fold-and-thrust regime followed by a transpressional regime where thrust and strike-slip faulting coexist, similarly to what is observed in the Shumagin region of the Aleutian Trench (Lewis et al., 1988). The present-day tectonic setting in the NAP is, in fact, very similar to those of the Aleutian Trench and Makran accretionary prism, where Lewis et al. (1988) and Platt et al. (1988) proposed three evolution stages: (1) folding along an axis perpendicular to the plate-convergence direction in the region, (2) thrust faulting in the direction of plate convergence, and (3) oblique strike-slip faulting along conjugate right-lateral and left-lateral faults. These conjugate strike-slip faults clearly post-date the initial fold-and-thrust geometry in both the Aleutian Trench and off- shore Makran, but evolved simultaneously with the major thrusts in the later stages of tectonic shortening. This suggests some overlap between the stages 2 and 3 previously described.

Some of the strike-slip faults in the study area (mainly fault F1) are associated with deeper inherited structures affecting the décollement (Tsuji et al., 2013). Most of the left-lateral NNW- to N-trending strike-slip faults are confined within the thrust anticlines and can be associated with a flat-and-ramp setting, where the lateral component of the oblique displacement of thrusts (flat) is transferred as left-lateral dis- placement in strike-slip faults (ramp) (Platt et al., 1988; Cunningham, 2005).

The presence of negative flower structures, when considered together with the branching of faults on seismic and attribute data (Fig. 4B and 8), suggests the occurrence of a transtensional regime (Sanderson and Marchini, 1984). As faults are very localized, and no major normal faults are observed in the study area, we interpret transtension as a consequence of the accommodation and partitioning of all transpressional deformation in the outer wedge of the NAP. The fact that there are no major normal faults within the outer wedge of the NAP, and that strike-slip is more common, indicates that strike-slip faulting is still accommodating the shortening of the outer wedge of the NAP, and that the maximum horizontal stress is, in fact, the direction of maximum compression (σ1) for the study area (Fig. 9A).

6. CONCLUSIONS

This work shows that the outer wedge of the NAP is a compressional region broadly affected by folding-and-thrusting and a secondary, but still important, strike-slip faulting regime. In particular, the study area is affected by three major types of structures: (1) a regional fold-and- thrust setting of synthetic thrusts, antithetic thrusts and corresponding anticlines; (2) localized conjugate families of strike-slip faults comprising left-lateral NNW- to N-trending faults and right-lateral WNW- to E-W trending faults. Within this latter family there is a major regional right-lateral strike-slip fault (F1) that separates two different structural domains. This strike-slip fault is associated with pre-existing structures affecting the décollement and the upper part of the outer wedge.

Maximum horizontal stress inferred from structures interpreted on seismic data is geometrically close to the convergence vector between the Eurasian and Philippine Sea Plates. Despite being clearly associated with past average stresses, maximum horizontal stress in the outer wedge may still represent the main direction of shortening in the NAP which is, at present, accommodated by strike-slip faults. In this rapidly evolving accretionary system, convergence was initially responsible for widespread compression in the NAP and formation of a fold-and-thrust setting, which progressed into a transpressional regime with thrust and strike-slip faulting occurring simultaneously, or in alternation. There is no evidence for a dominant extensional regime, or a transition from a shallow extensional regime to a deeper compressional or strike-slip regime. Extensional structures and stress decoupling are only visible in regions with significant sediment cover, thus comprising the superficial expression of deeper transpressional tectonics or localized areas of larger structural complexity. The recognition of a transpressional regime operating in the outer wedge of the NAP at present has a significant impact in the stress distribution and consequent accommodation of strain offshore Nankai.

ACKNOWLEDGMENTS

This research used seismic data from the Kumano Transect collected by PGS and processed by CGG and IFREE/JAMSTEC. Schlumberger is acknowledged for providing Petrel® software and licenses to the 3D Seismic Lab. We thank the reviewers and editor for their constructive comments, which greatly improved an early version of this manuscript.

REFERENCES CITED

Alves, T.M., et al., 2013. Erosional features as indicators of thrust fault activity (Nankai Trough, Japan). Mar. Geol. 356, 5–18. http://dx.doi.org/10.1016/j.margeo.2013.07. 011.

Anderson, E.M., 1905. The dynamics of faulting. Transactions of the Edinburgh Geological Society 8 (3), 387–402. http://dx.doi.org/10.1144/transed.8.3.387.

Bangs, N.L.B., Moore, G.F., Gulick, S.P.S., Pangborn, E.M., Tobin, H.J., Kuramoto, S., Taira, A., 2009. Broad, weak regions of the Nankai Megathrust and implications for shallow coseismic slip. Earth Planet. Sci. Lett. 284, 44–49. http://dx.doi.org/10. 1016/j.epsl.2009.04.026.

Boston, B., Moore, G.F., Jurado, M.J., Sone, H., 2016. Deformation of the Nankai Trough inner accretionary prism: the role of inherited structures. Geochemistry Geophysics Geosystem 17, 485–500. http://dx.doi.org/10.1002/2015GC006185.

Burchfiel, B.C., Royden, L.H., 1985. North-south extension within the convergent Himalayan region. Geology 13 (10), 679–682. http://dx.doi.org/10.1130/0091- 7613(1985)13<679:NEWTCH>2.0.CO;2.

Byrne, D.E., Wang, W.H., Davis, D.M., 1993. Mechanical role of backstops in the growth of forearcs. Tectonics 12 (1), 123–144. http://dx.doi.org/10.1029/92TC00618. Byrne, T.B., Lin, W., Tsutsumi, A., Yamamoto, Y., Lewis, J.C., Kanagawa, K., Kitamura, Y., Yamaguchi, A., Kimura, G., 2009. Anelastic strain recovery reveals extension across SW Japan subduction zone. Geophys. Res. Lett. 36 (23). http://dx.doi.org/10.1029/ 2009GL040749.

Chang, C., Song, I., 2016. Present-day stress states underneath the Kumano basin to 2 km below seafloor based on borehole wall failures at IODP site C0002, Nankai accre- tionary wedge. Geochem. Geophys. Geosyst. 17. http://dx.doi.org/10.1002/ 2016GC006562.

Chopra, S., Marfurt, K.J., 2005. Seismic attributes—a historical perspective. Geophysics 70 (5), 3SO–28SO. http://dx.doi.org/10.1190/1.2098670.

Chopra, S., Marfurt, K., 2007a. Curvature attribute applications to 3D surface seismic data. Lead. Edge 26 (4), 404–414. http://dx.doi.org/10.1190/1.2723201.

Chopra, S., Marfurt, K.J., 2007b. Volumetric curvature attributes for fault/fracture characterization. First Break 25 (7), 35–46. http://dx.doi.org/10.3997/1365–2397. 2007019.

Cunningham, D., 2005. Active intracontinental transpressional mountain building in the Mongolian Altai: defining a new class of orogeny. Earth Planet. Sci. Lett. 240 (2), 436–444. http://dx.doi.org/10.1016/j.epsl.2005.09.013.

Dahlen, F.A., Suppe, J., Davis, D., 1984. Mechanics of fold-and-thrust belts and accre- tionary wedges: cohesive Coulomb theory. J. Geophys. Res. Solid Earth 89 (B12), 10087–10101. http://dx.doi.org/10.1029/JB089iB12p10087.

Davis, D., Suppe, J., Dahlen, F.A., 1983. Mechanics of fold-and-thrust belts and accre- tionary wedges. J. Geophys. Res. Solid Earth 88 (B2), 1153–1172. http://dx.doi.org/ 10.1029/JB088iB02p01153.

DeMets, C., Gordon, R.G., Argus, D.F., 2010. Geologically current plate motions. Geophys. J. Int. 181 (1), 1–80. http://dx.doi.org/10.1111/j.1365-246X.2009.04491.x.

Expedition 315 Scientists, 2009. Expedition 315 Site C0001: Proceedings of the Integrated Ocean Drilling Program. vol. 314/315/316http://dx.doi.org/10.2204/iodp.proc. 314315316.123.2009.

Expedition 316 Scientists, 2009. Expedition 316 Site C0006. In: Kinoshita, M., Tobin, H., Ashi, J., Kimura, G., Lallemant, S., Screaton, E.J., Curewitz, D., Masago, H., Moe, K.T. (Eds.), The Expedition 314/315/316 Scientists, Proc. IODP, 314/315/316, http://dx. doi.org/10.2204/iodp.proc.314315316.134.2009.

Expedition 333 Scientists, 2012. Site C0018. In: Henry, P., Kanamatsu, T., Moe, K. (Eds.), The Expedition 333 Scientists, Proc. IODP, 333. Integrated Ocean Drilling Program Management International, Inc., Tokyo. http://dx.doi.org/10.2204/iodp.proc.333. 103.2012.

Gulick, S.P.S., Bangs, N.L.B., Shipley, T.H., Nakamura, Y., Moore, G., Kuramoto, S., 2004. Three-dimensional architecture of the Nankai accretionary prism's imbricate thrust zone off Cape Muroto, Japan: prism reconstruction via en echelon thrust propagation. J. Geophys. Res. Solid Earth 109 (B2), 1978–2012. http://dx.doi.org/10.1029/ 2003JB002654.

Hancock, P.L., 1985. Brittle microtectonics: principles and practice. J. Struct. Geol. 7 (3), 437–457. http://dx.doi.org/10.1016/0191-8141(85)90048-3.

Harding, T.P., 1985. Seismic characteristics and identification of negative flower struc- tures, positive flower structures, and positive structural inversion. AAPG Bull. 69 (4), 582–600.

Huffman, K.A., Saffer, D.M., 2016. In situ stress magnitudes at the toe of the Nankai trough accretionary prism, offshore Shikoku Island, Japan. J. Geophys. Res. Solid Earth 121, 1202–1217. http://dx.doi.org/10.1002/2015JB012415.

Ismat, Z., 2015. What can the dihedral angle of conjugate-faults tell us? J. Struct. Geol. 73, 97–113. http://dx.doi.org/10.1016/j.jsg.2015.02.008.

Kamei, R., Pratt, R.G., Tsuji, T., 2012. Waveform tomography imaging of a megasplay fault system in the seismogenic Nankai subduction zone. Earth Planet. Sci. Lett. 317, 343–353. http://dx.doi.org/10.1016/j.epsl.2011.10.042.

Kimura, G., Kitamura, Y., Hashimoto, Y., Yamaguchi, A., Shibata, T., Ujiie, K., Okamoto, S.Y., 2007. Transition of accretionary wedge structures around the up-dip limit of the seismogenic subduction zone. Earth Planet. Sci. Lett. 255 (3), 471–484. http://dx.doi. org/10.1016/j.epsl.2007.01.005.

Kimura, G., Moore, G.F., Strasser, M., Screaton, E., Curewitz, D., Streiff, C., Tobin, H., 2011. Spatial and temporal evolution of the megasplay fault in the Nankai Trough. Geochem. Geophys. Geosyst. 12 (3). http://dx.doi.org/10.1029/2010GC003335.

Kodaira, S., Iidaka, T., Kato, A., Park, J.O., Iwasaki, T., Kaneda, Y., 2004. High pore fluid pressure may cause silent slip in the Nankai Trough. Science 304 (5675), 1295–1298. http://dx.doi.org/10.1126/science.1096535.

Kodaira, S., Hori, T., Ito, A., Miura, S., Fujie, G., Park, J.-O., Baba, T., Sakaguchi, H., Kaneda, Y., 2006. A cause of rupture segmentation and synchronization in the Nankai trough revealed by seismic imaging and numerical simulation. J. Geophys. Res. 111. http://dx.doi.org/10.1029/2005JB004030.

Le Pichon, X., Kobayashi, K., Crew, K.N.S., 1992. Fluid venting activity within the eastern Nankai Trough accretionary wedge: a summary of the 1989 Kaiko-Nankai results. Earth Planet. Sci. Lett. 109 (3), 303–318. http://dx.doi.org/10.1016/0012-821X(92) 90094-C.

Le Pichon, X., Wmant, S., Tokuyama, H., Thoue, F., Huchon, P., Henry, P., 1996. Structure and evolution of the backstop in the eastern Nankai trough area (Japan): implications for the soon-to-come Tokai earthquake. Island Arc 5 (4), 440–454. http://dx.doi.org/ 10.1111/j.1440-1738.1996.tb00164.x.

Lewis, S.D., Ladd, J.W., Bruns, T.R., 1988. Structural development of an accretionary prism by thrust and strike-slip faulting: Shumagin region, Aleutian Trench. Geol. Soc. Am. Bull. 100, 767–782.

Lewis, J.C., Byrne, T.B., Kanagawa, K., 2013. Evidence for mechanical decoupling of the upper plate at the Nankai subduction zone: constraints from core-scale faults at NantroSEIZE Sites C0001 and C0002. Geochem. Geophys. Geosyst. 14 (3), 620–633. http://dx.doi.org/10.1029/2012GC004406.

Lin, W., Byrne, T.B., Kinoshita, M., McNeill, L.C., Chang, C., Lewis, J.C., Yamamoto, Y., Saffer, D.M., Casey Moore, J., Wu, H.-Y., Tsuji, T., Yamada, Y., Conin, M., Saito, S., Ito, T., Tobin, H.J., Kimura, G., Kanagawa, K., Ashi, J., Underwood, M.B., Kanamatsu, T., 2015. Distribution of stress state in the Nankai subduction zone, southwest Japan and a comparison with Japan Trench. Tectonophysics 692, 120–130. http://dx.doi. org/10.1016/j.tecto.2015.05.008.

MacKay, M.E., Moore, G.F., Cochrane, G.R., Casey Moore, J., Kulm, LaVerne D., 1992. Landward vergence and oblique structural trends in the Oregon margin accretionary prism: Implications and effect on fluid flow. Earth Planet. Sci. Lett. 109 (3–4), 477–491.

Mai, H.T., Marfurt, K.J., Chávez-Pérez, S., 2009. Coherence and volumetric curvatures and their spatial relationship to faults and folds, an example from Chicontepec basin, Mexico. In: SEG Technical Program Expanded Abstracts. vol. 2009. pp. 1063–1067. http://dx.doi.org/10.1190/1.3255033.

Martin, K.M., Gulick, S.P.S., Bangs, N.L.B., Moore, G.F., Ashi, J., Park, J.-O., Kuramoto, S., Taira, A., 2010. Possible strain partitioning structure between the Kumano fore-arc basin and the slope of the Nankai Trough accretionary prism. Geochem. Geophys. Geosyst. 11http://dx.doi.org/10.1029/2009GC002668. (Q0AD02).

McKenzie, D., Jackson, J., 1986. A block model of distributed deformation by faulting. J. Geol. Soc. 143 (2), 349–353. http://dx.doi.org/10.1144/gsjgs.143.2.0349.

Miyazaki, S.I., Heki, K., 2001. Crustal velocity field of southwest Japan: subduction and arc-arc collision. J. Geophys. Res. Solid Earth 106 (B3), 4305–4326. http://dx.doi. org/10.1029/2000JB900312.

Moore, Gregory F., Taira, A., Klaus, A., Becker, L., Boeckel, B., Cragg, B.A., Dean, A., Fergusson, C.L., Henry, P., Hirano, S., Hisamitsu, T., Hunze, S., Kastner, M., Maltman, A.J., Morgan, J.K., Murakami, Y., Saffer, D.M., Sánchez-Gómez, M., Screaton, E.J., Smith, D.C., Spivack, J.A., Steurer, J., Tobin, H.J., Ujiie, K., Underwood, M.B., Wilson, M., 2001. New insights into deformation and fluid flow processes in the Nankai Trough accretionary prism: results of ocean drilling program leg 190. Geochem. Geophys. Geosyst. 2.

Moore, G.F., Bangs, N.L., Taira, A., Kuramoto, S., Pangborn, E., Tobin, H.J., 2007. Three- dimensional splay fault geometry and implications for tsunami generation. Science 318 (5853), 1128–1131. http://dx.doi.org/10.1126/science.1147195.

Moore, G.F., Park, J.-O., Bangs, N.L., Gulick, S.P., Tobin, H.J., Nakamura, Y., Sato, S., Tsuji, T., Yoro, T., Tanaka, H., Uraki, S., Kido, Y., Sanada, Y., Kuramoto, S., Taira, A., 2009. Structural and seismic stratigraphic framework of the NanTroSEIZE Stage 1 transect. In: Kinoshita, M., Tobin, H., Ashi, J., Kimura, G., Lallemant, S., Screaton, E.J., Curewitz, D., Masago, H., Moe, K.T., the Expedition 314/315/316 Scientists (Eds.), Proc. IODP, 314/315/316. (Integrated Ocean Drilling Program Management International, Inc.), Washington, DC. http://dx.doi.org/10.2204/iodp.proc. 314315316.102.2009.

Moore, G.F., Boston, B.B., Sacks, A.F., Saffer, D.M., 2013. Analysis of normal fault po- pulations in the Kumano Forearc Basin, Nankai Trough, Japan: 1. Multiple orienta- tions and generations of faults from

3-D coherency mapping. Geochem. Geophys. Geosyst. 14 (6), 1989–2002. http://dx.doi.org/10.1002/ggge.20119.

Moore, G.F., Boston, B.B., Strasser, M., Underwood, M.B., Ratliff, R.A., 2015. Evolution of tectono-sedimentary systems in the Kumano Basin, Nankai trough forearc. Mar. Pet.

Geol. 67, 604–616. http://dx.doi.org/10.1016/j.marpetgeo.2015.05.032. Obana, K., Kodaira, S., Kaneda, Y., 2005. Seismicity in the incoming/subducting

Philippine Sea plate off the Kii Peninsula, central Nankai trough. J. Geophys. Res.

110. http://dx.doi.org/10.1029/2004JB003487.

Park, J.O., Tsuru, T., Kaneda, Y., Kono, Y., Kodaira, S., Takahashi, N., Kinoshita, H., 1999.

A subducting seamount beneath the Nankai accretionary prism off Shikoku, south- western Japan. Geophys. Res. Lett. 26 (7), 931–934. http://dx.doi.org/10.1029/ 1999GL900134.

Park, J.O., Tsuru, T., Kodaira, S., Cummins, P.R., Kaneda, Y., 2002. Splay fault branching along the Nankai subduction zone. Science 297 (5584), 1157–1160. http://dx.doi. org/10.1126/science.1074111.

Park, J.-O., Fujie, G., Wijerathne, L., Hori, T., Kodaira, S., Fukao, Y., Moore, G.F., Bangs, N.L., Kuramoto, S., Taira, A., 2010. A low-velocity zone with weak reflectivity along the Nankai subduction zone. Geology 38 (3), 283–286. http://dx.doi.org/10.1130/ G30205.1.

Platt, J.P., Leggett, J.K., Alam, S., 1988. Slip vectors and fault mechanics in the Makran accretionary wedge, southwest Pakistan. J. Geophys. Res. Solid Earth 93 (B7), 7955–7973.

Ramsey, J.M., Chester, F.M., 2004. Hybrid fracture and the transition from extension fracture to shear fracture. Nature 428 (6978), 63–66. http://dx.doi.org/10.1038/ nature02333.

Roberts, A., 2001. Curvature attributes and their application to 3 D interpreted horizons. First Break 19 (2), 85–100. http://dx.doi.org/10.1046/j.0263-5046.2001.00142.x.

Sanderson, D.J., Marchini, W.R.D., 1984. Transpression. J. Struct. Geol. 6 (5), 449–458. http://dx.doi.org/10.1016/0191-8141(84)90058-0.

Shelton, J.W., 1984. Listric normal faults: an illustrated summary. AAPG Bull. 68 (7), 801–815.

Strasser, M., Moore, G.F., Kimura, G., Kopf, A.J., Underwood, M.B., Guo, J., Screaton, E.J., 2011. Slumping and mass transport deposition in the Nankai fore arc: evidence from IODP drilling and 3-D reflection seismic data. Geochem. Geophys. Geosyst. 12 (5). http://dx.doi.org/10.1029/2010GC003431.

Strasser, M., Dugan, B., Kanagawa, K., Moore, G.F., Toczko, S., Maeda, L., The Expedition 338 Scientists, 2014. Site C0018: Proceedings of the Integrated Ocean Drilling Program. vol. 338. pp. 2. http://dx.doi.org/10.2204/iodp.proc.338.105.2014.

Takahashi, N., Amano, H., Hirata, K., Kinoshita, H., Lallemant, S., Tokuyama, H., Tamamoto, F., Taira, A., Suyehiro, K., 2002. Faults configuration around the eastern Nankai trough deduced by multichannel seismic profiling. Mar. Geol. 187 (1), 31–46. http://dx.doi.org/10.1016/S0025-3227(02)00243-8.

Tobin, H.J., Kinoshita, M., 2006. NanTroSEIZE: the IODP Nankai Trough seismogenic zone experiment. Sci. Drill. 2 (2), 23–27. http://dx.doi.org/10.2204/iodp.sd.2.06. 2006.

Tsuji, T., Tokuyama, H., Costa Pisani, P., Moore, G., 2008. Effective stress and pore pressure in the Nankai accretionary prism off the Muroto Peninsula, southwestern Japan. J. Geophys. Res. Solid Earth 113 (B11). http://dx.doi.org/10.1029/ 2007JB005002.

Tsuji, T., Park, J.-O., Moore, G., Kodaira, S., Fukao, Y., Kuramoto, S., Bangs, N., 2009. Intraoceanic thrusts in the Nankai Trough off the Kii Peninsula: implications for in- traplate earthquakes. Geophys. Res. Lett. 36, L06303. http://dx.doi.org/10.1029/ 2008GL036974.

Tsuji, T., Kodaira, S., Ashi, J., Park, J.O., 2013. Widely distributed thrust and strike-slip faults within subducting oceanic crust in the Nankai Trough off the Kii Peninsula, Japan. Tectonophysics 600, 52–62. http://dx.doi.org/10.1016/j.tecto.2013.03.014.

Tsuji, T., Ashi, J., Ikeda, Y., 2014. Strike-slip motion of a mega-splay fault system in the Nankai oblique subduction zone. Earth, Planets Space 66 (1), 1–14. http://dx.doi. org/10.1186/1880-5981-66-120.

Van Tuyl, J., Alves, T.M., Moore, G.F., 2015. Strain decoupling reveals variable seismo- genic risk in SE Japan (Nankai Trough). Geochem. Geophys. Geosyst. 16 (7), 2025–2037. http://dx.doi.org/10.1002/2015GC005778.

Wang, K., Hu, Y., 2006. Accretionary prisms in subduction earthquake cycles: The theory of dynamic Coulomb wedge. J. Geophys. Res. Solid Earth 111 (B6). http://dx.doi. org/10.1029/2005JB004094.

Wu, H.Y., Chan, C.H., Kinoshita, M., Saito, S., 2013. Stress field observation and modeling from the NanTroSEIZE scientific drillings in the Nankai Trough system, SW Japan. Tectonophysics 600, 99–107. http://dx.doi.org/10.1016/j.tecto.2013.04.009.

FIGURES

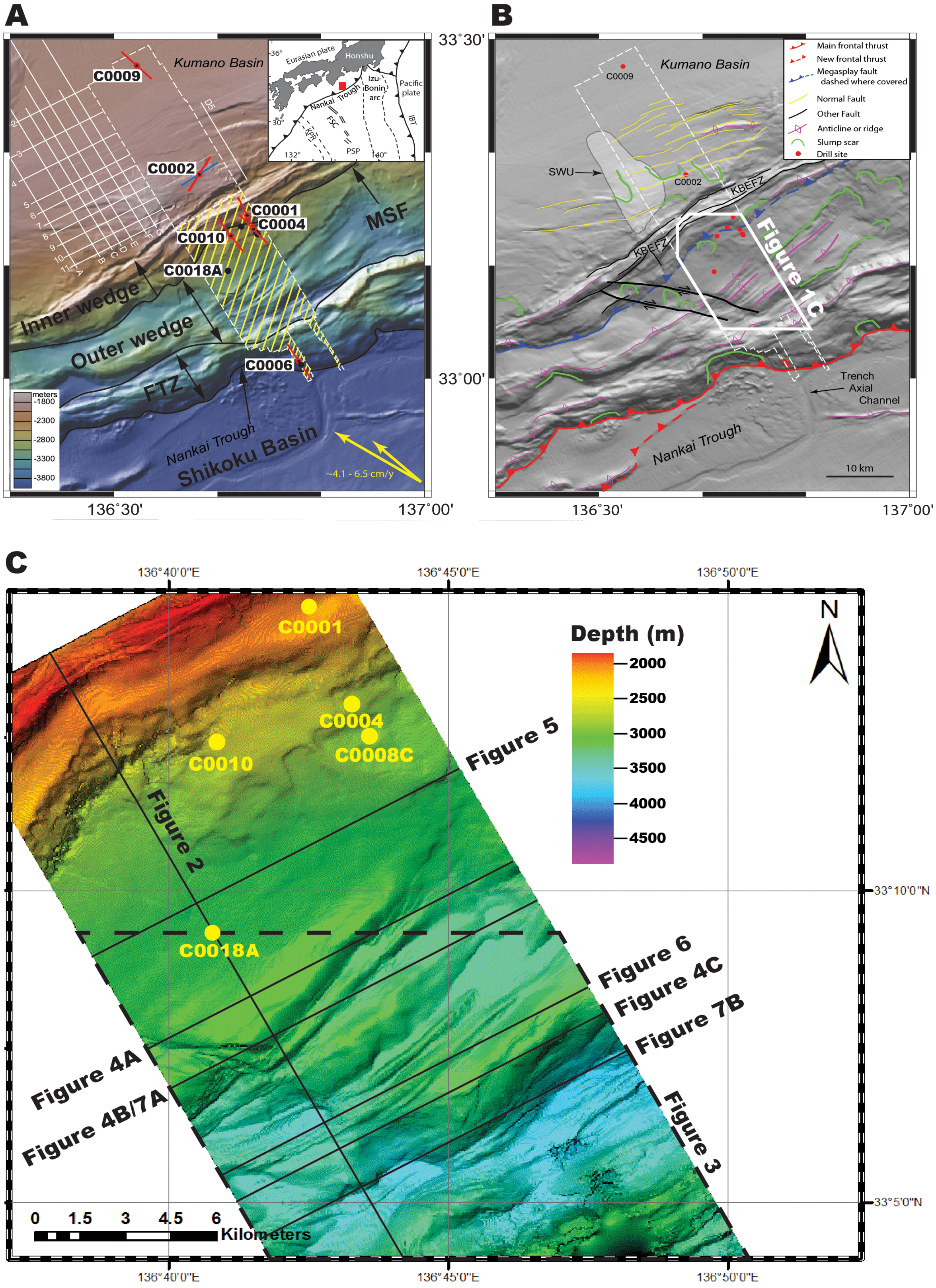
A
B
C
33°30'
33°00'
136°30'
137°00'
Kumano Basin
C0009
C0002
C0001
C0004
C0010
C0018A
C0006
D5
MSF
Inner wedge
Outer wedge
FTZ
Nankai Trough
Shikoku Basin
~4.1 - 6.5 cm/y
meters
-1800
-2300
-2800
-3300
-3800
Eurasian plate
Honshu
Izu-Bonin arc
Pacific plate
Nankai Trough
FSC
KPR
PSP
IBT
36°
30°
132°
140°
Main frontal thrust
New frontal thrust
Megasplay fault dashed where covered
Normal Fault
Other Fault
Anticline or ridge
Slump scar
Drill site
SWU
KBEFZ
Figure 1C
Trench Axial Channel
10 km
136°40'0"E
136°45'0"E
136°50'0"E
33°10'0"N
33°5'0"N
Depth (m)
2000
2500
3000
3500
4000
4500
N
C0008C
Figure 2
Figure 5
Figure 6
Figure 4C
Figure 7B
Figure 4A
Figure 4B/7A
Figure 3
0
1.5
3
4.5
6
Kilometers

Fig. 1. A) Relief map of the Kumano Basin region of the Nankai Trough as modified from Moore et al. (2013). The figure shows the location of the 3D seismic volume (white dashed box), maximum horizontal stress directions (red lines and blue line), the location of JAMSTEC 2-D seismic lines (white lines) and convergence vectors between the Philippine Sea Plate and Japan (yellow arrows). Also highlighted in the figure are the study area (yellow lines) and distinct tectonic regions in the NAP as shown in Kimura et al. (2011). The inset shows a regional tectonic map with the present day configuration of the Nankai Trough. MSF - Megasplay Fault; ITZ - Imbricate Thrust Zone; FTZ - Frontal Thrust Zone; KPR- Kyushu-Palau Ridge; FSC - fossil spreading center; PSP - Philippine Sea Plate; IBT - Izu-Bonin Trench. Red box shows the location of the study area in SE Japan. B) Tectonic interpretation from Moore et al. (2013) showing the area interpreted in Fig. 1C. KBEFZ = Kumano Basin Edge Fault Zone; SWU = southwestern uplift. C) Bathymetric map derived from the Kumano 3D seismic volume showing the direction of seismic profiles in this paper and IODP Sites C0001, C0004, C0008C, C0010 and C0018A. The study area comprises the southern limit of the Kumano Transect, up to the MSFZ.

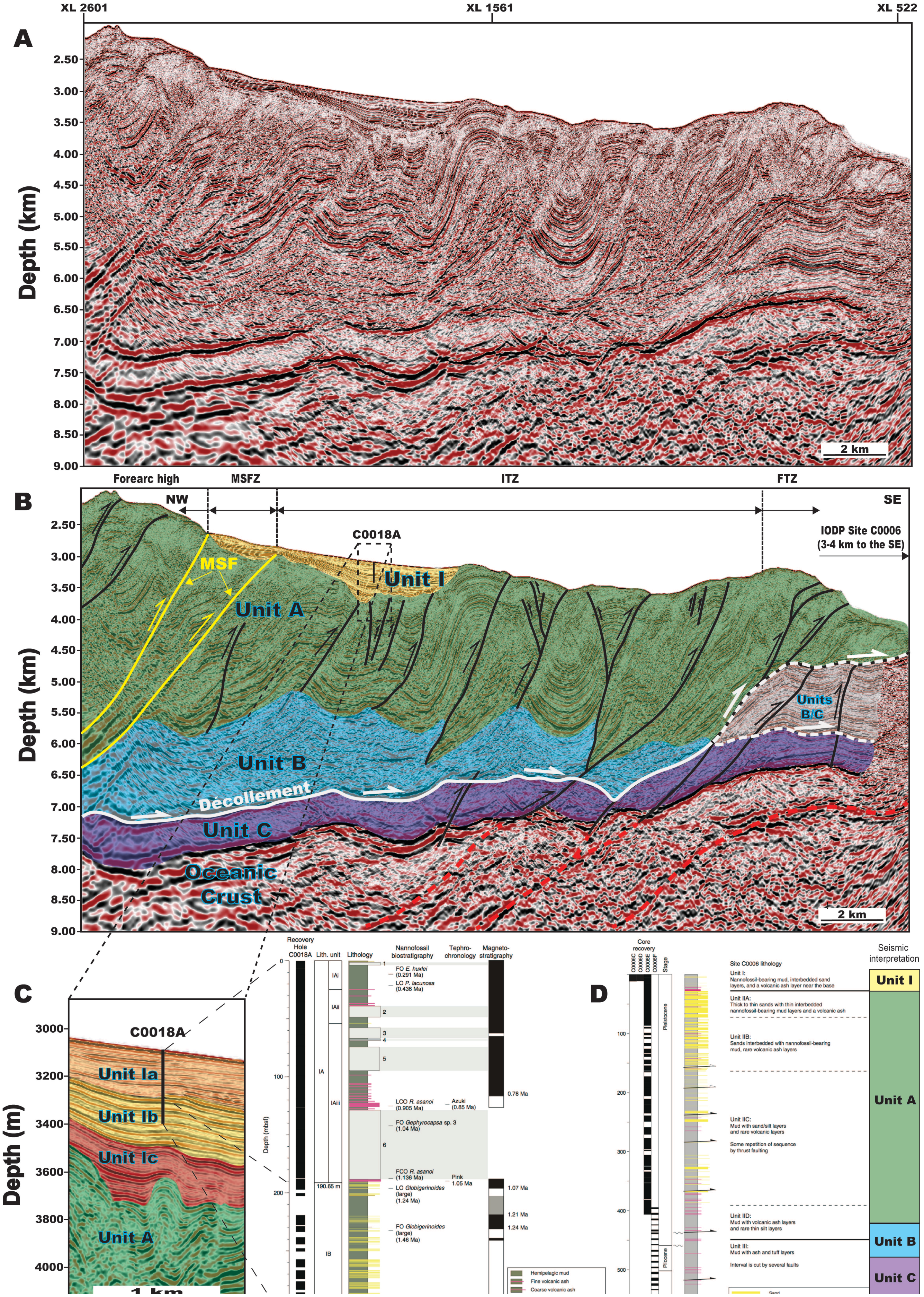
XL 2601
XL 1561
XL 522
A
Depth (km)
2.50
3.00
3.50
4.00
4.50
5.00
5.50
6.00
6.50
7.00
7.50
8.00
8.50
9.00
2 km
Forearc high
MSFZ
ITZ
FTZ
B
NW
SE
C0018A
IODP Site C0006
(3-4 km to the SE)
MSF
Unit I
Unit A
Units B/C
Unit B
Décollement
Unit C
Oceanic Crust
2 km
C
Depth (m)
3000
3200
3400
3600
3800
4000
C0018A
Unit Ia
Unit Ib
Unit Ic
Unit A
1 km
Recovery Hole C0018A
Lith. unit
Lithology
Nannofossil biostratigraphy
Tephro-chronology
Magneto-stratigraphy
Depth (mbsf)
0
100
200
IA
IAi
IAii
IAiii
IB
190.65 m
1
2
3
4
5
6
FO E. huxlei (0.291 Ma)
LO P. lacunosa (0.436 Ma)
LCO R. asanoi (0.905 Ma)
FO Gephyrocapsa sp. 3 (1.04 Ma)
FCO R. asanoi (1.136 Ma)
LO Globigerinoides (large) (1.24 Ma)
FO Globigerinoides (large) (1.46 Ma)
Azuki (0.85 Ma)
Pink 1.05 Ma
0.78 Ma
1.07 Ma
1.21 Ma
1.24 Ma
Hemipelagic mud
Fine volcanic ash
Coarse volcanic ash
D
Core recovery
C0006C
C0006D
C0006E
C0006F
Stage
Pleistocene
Pliocene
100
200
300
400
500
Site C0006 lithology
Unit I:
Nannofossil-bearing mud, interbedded sand layers, and a volcanic ash layer near the base
Unit IIA:
Thick to thin sands with thin interbedded nannofossil-bearing mud layers and a volcanic ash
Unit IIB:
Sands interbedded with nannofossil-bearing mud, rare volcanic ash layers
Unit IIC:
Mud with sand/silt layers and rare volcanic layers
Some repetition of sequence by thrust faulting
Unit IID:
Mud with volcanic ash layers and rare thin silt layers
Unit III:
Mud with ash and tuff layers
Interval is cut by several faults
Sand
Seismic interpretation
Unit I
Unit A
Unit B
Unit C

Fig. 2. A & B) Depth-migrated seismic profile (Inline 2315) across thrust-and-fold structures in the NAP. The figures also show interpreted (colored and shaded) tectono-stratigraphic units and the location of IODP Site C0018A. Unit I (yellow) represents relatively undeformed slope sediment (Expedition 315 Scientists, 2009; Kimura et al., 2011; Alves et al., 2013; Strasser et al., 2014), whereas Units A (green), B (blue), C (purple) and oceanic crust (colorless) are interpreted based on Park et al. (2010). IODP Site C0006 is 3–4 km distant from the SE end of the seismic profile, meaning that the interpreted seismic units show lateral continuity with the tectono-stratigraphic units shown in Fig. 2D for IODP Site C0006, further southeast. The area labeled as seismic units B/C is open to interpretation as the seismic resolution significantly decreases further SE. (black lines – major thrust and back-thrust faults; arrows – vergence of anticlines and thrusts; white line – décollement fault; dashed white lines – possible décollement paths; dashed red lines – possible faults within the subducted oceanic crust; yellow lines – splays of the MSFZ; MSFZ – Megasplay Fault Zone; ITZ – Imbricate Thrust Zone; FTZ – Frontal Thrust Zone). C) Close-up of IODP well C0018A highlighting the subdivision of Unit I in Units Ia, Ib and Ic based on Strasser et al. (2014). D) Well log from IODP Site C0006 (Expedition 316 Scientists, 2009) tied to the seismic units interpreted in this work. According to Expedition 316 Scientists (2009), Unit III is consistent with deposition in the Shikoku Basin.

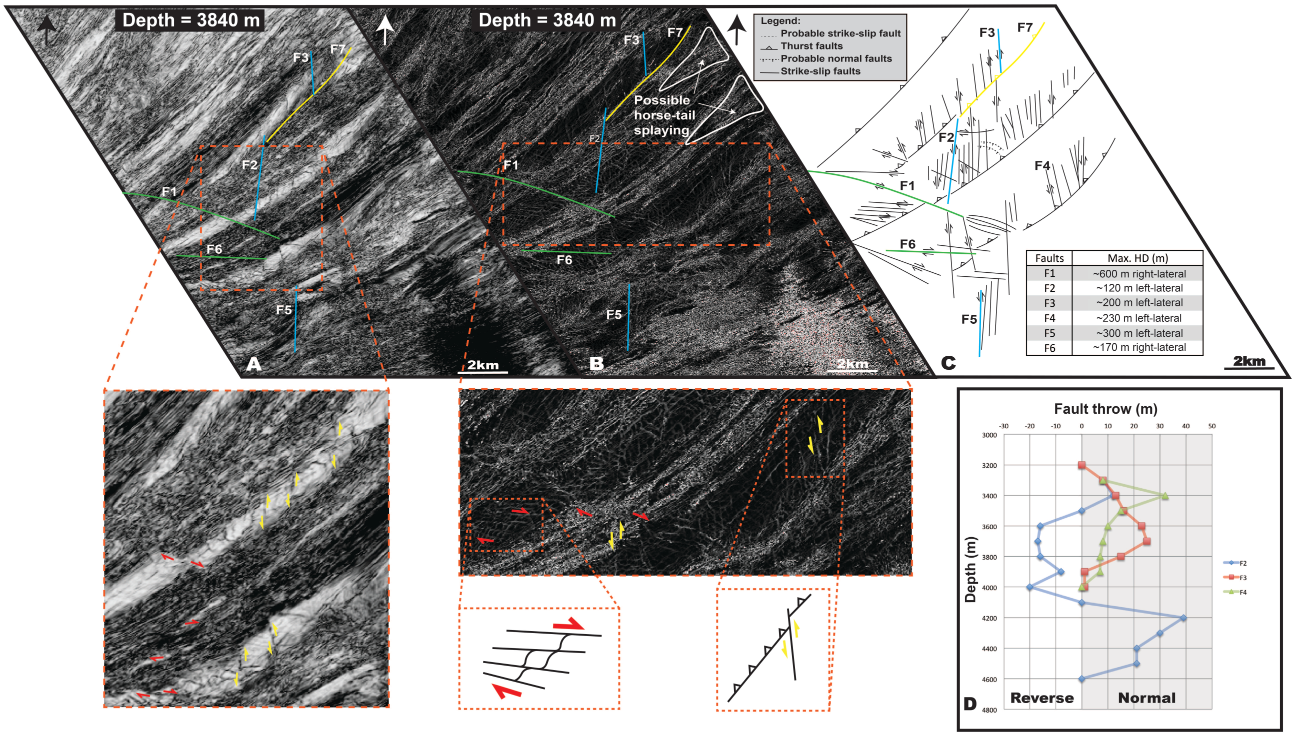

Faults	Max. HD (m)
F1	~600 m right-lateral
F2	~120 m left-lateral
F3	~200 m left-lateral
F4	~230 m left-lateral
F5	~300 m left-lateral
F6	~170 m right-lateral

Fig. 3. A & B) Coherence and maximum curvature maps (at a depth of 3840 m) with corresponding zoomed insets showing main structural lineaments and interpreted faults. Red half-arrows – relative right-lateral movement; yellow half-arrows – relative left-lateral movement C) Schematic interpretation of the geometry and kinematics of main faults based on coherence maps, volumetric curvature maps and seismic data. Lower right-hand corner: table showing the maximum horizontal displacement (max. HD) and the type of horizontal displacement in faults F1 to F6. Three families of faults were identified: NE-trending thrusts (yellow), NNW- to N-trending left-lateral strike-slip faults (blue) and WNW- to E-W right- lateral strike-slip faults (green). D) Graph showing the amount and nature of throw (or vertical separation) in three NNW- to N-trending faults (F2 to F4). Throws of faults F2, F3 and F4 were measured every 50 m in their middle part and along their full height. The graph shows a sharp variation in the throw of the faults, and type of vertical offset, providing evidence for horizontal motion. Furthermore, in most faults lateral slip is much larger than vertical (dip) slip.

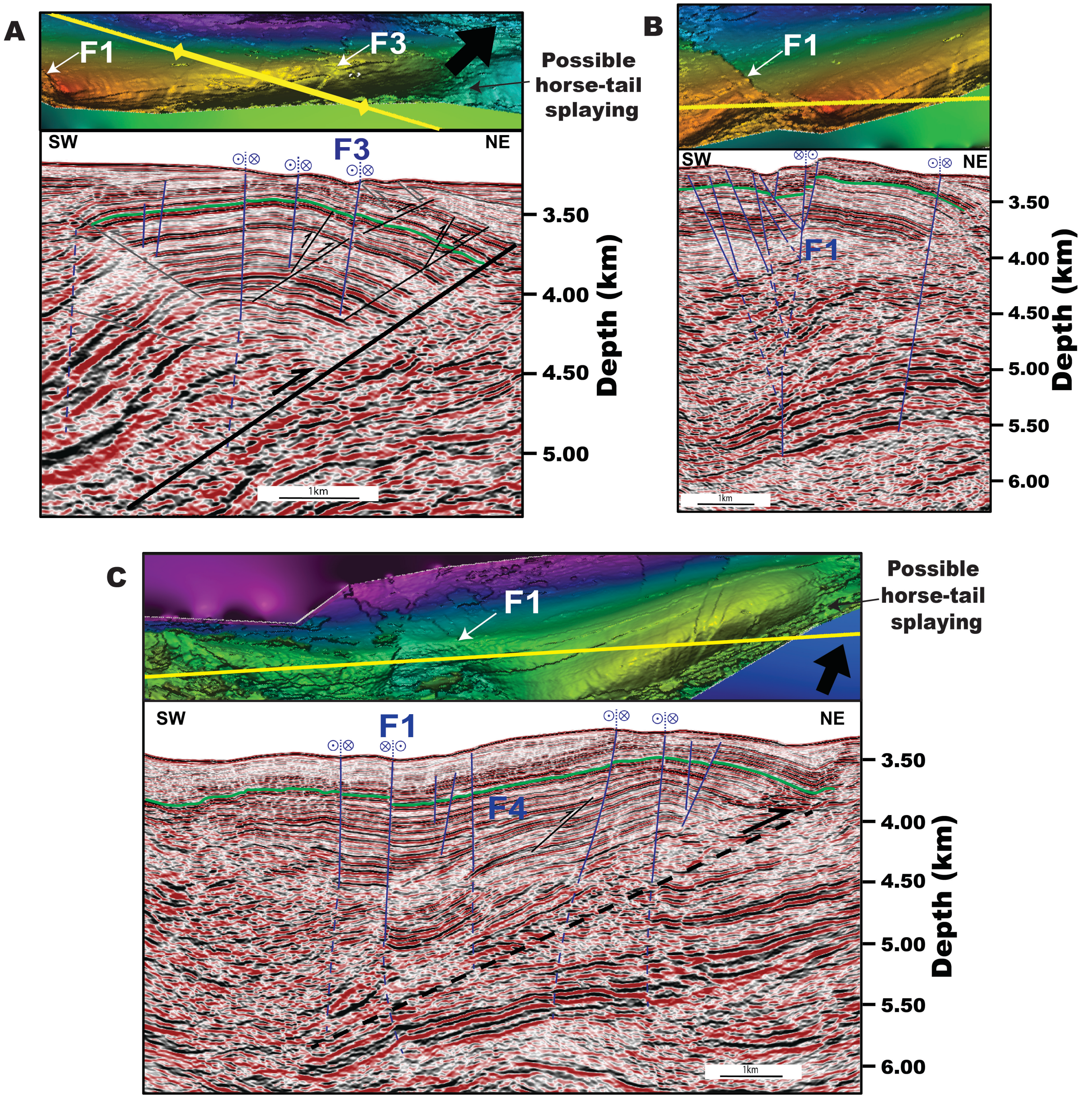

Fig. 4. In this figure, the maps on top show detailed seismic horizons that follow the main thrust anticlines identified in Fig. 3. The seismic profiles below intersect the main thrust anticlines and highlight the geometry of interpreted faults and their kinematics within Unit A. Yellow line - location of the seismic profile below; Green line – seismic horizon of map view above; Blue – strike-slip fault; Black – thrust fault; Grey – antithetic thrust fault. Dashed line – probable fault. A) Seismic crossline 1671. Strike-slip faults intersect and displace primary thrust faults in this profile, whereas larger scale thrusts do not

seem to be affected. B) Seismic crossline 1571. Negative flower structure likely associated with local transtension. C) Seismic crossline 1251. Right-lateral and left-lateral strike-slip faults with variable throws. Some faults are observed on both the hanging-wall and footwall of the thrust anticlines.

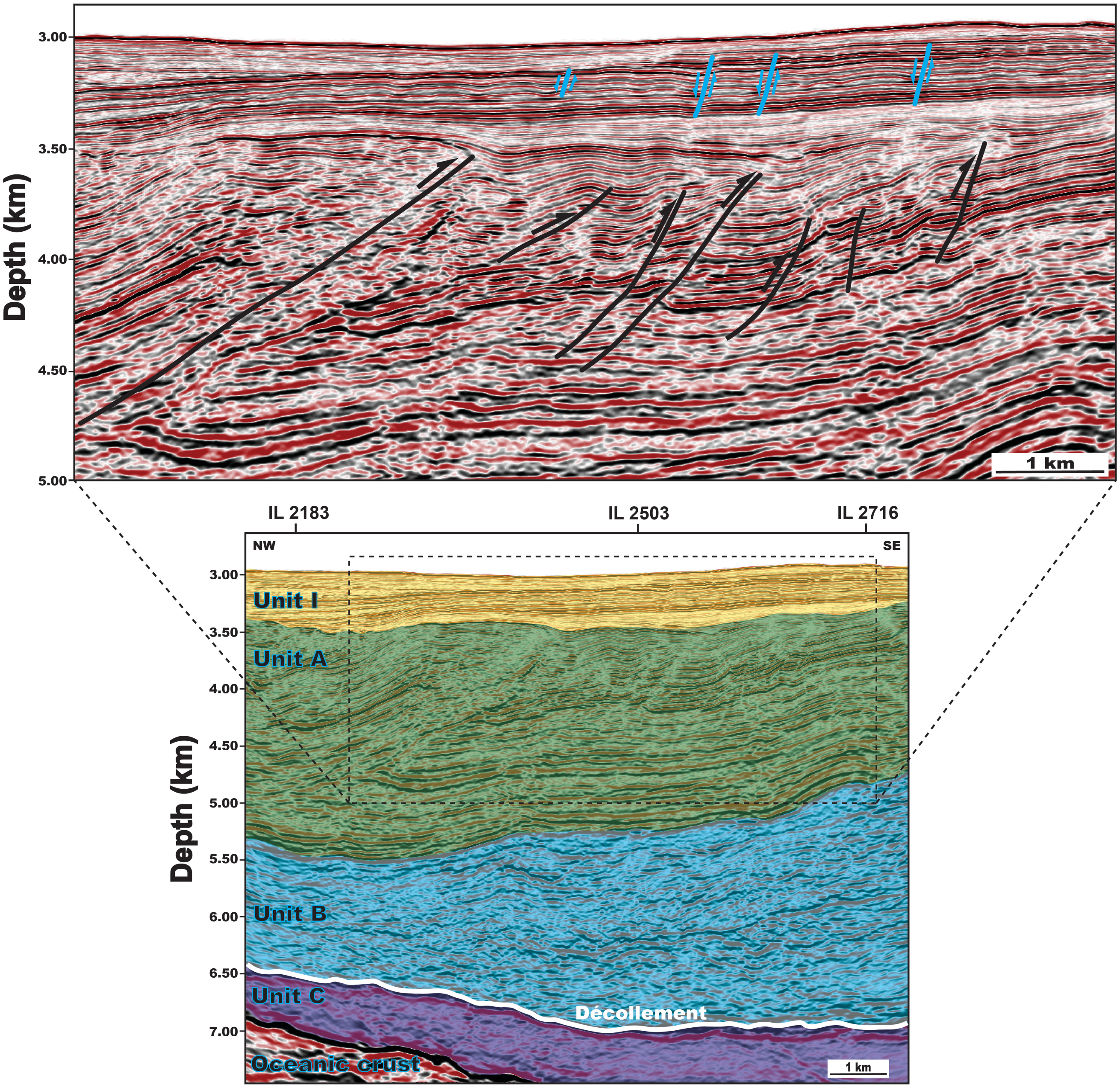

Fig. 5. Depth-migrated seismic profile (crossline 1920) across the landward section of the outer wedge of the NAP showing the tectono-stratigraphic units described in Fig. 2. The inset above shows thrust faults (black lines) within Unit A, where some reach the contact between Units I and A. A few normal faults

(blue lines) within Unit I are associated with the gravitational collapse/stress readjustment that results from local tectonic uplift caused by the deeper thrusts.

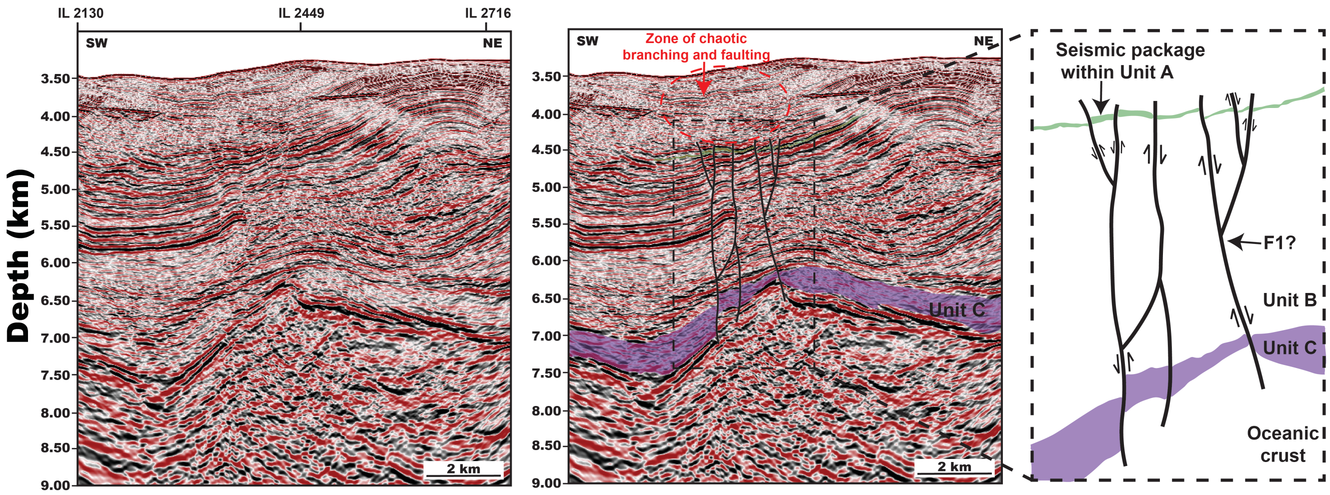

Fig. 6. Depth-migrated seismic profile (crossline 1320; with original profile on the left and interpreted section on the right) showing irregular relative displacements between blocks that are horizontally and vertically adjacent. This disagreement among fault displacements cannot be explained by pure extensional or compressional regimes. Black arrows show the relative displacement between adjacent blocks of strike-slip faults (black lines). Dashed red ellipse highlights a shallower zone of random fractures with minor displacement(s), probably branching from major faults. Some of these minor branches reach the sea floor, affecting the local bathymetry. Green horizon – a seismic horizon of Unit A; Purple horizon – Unit C; IL - Inline

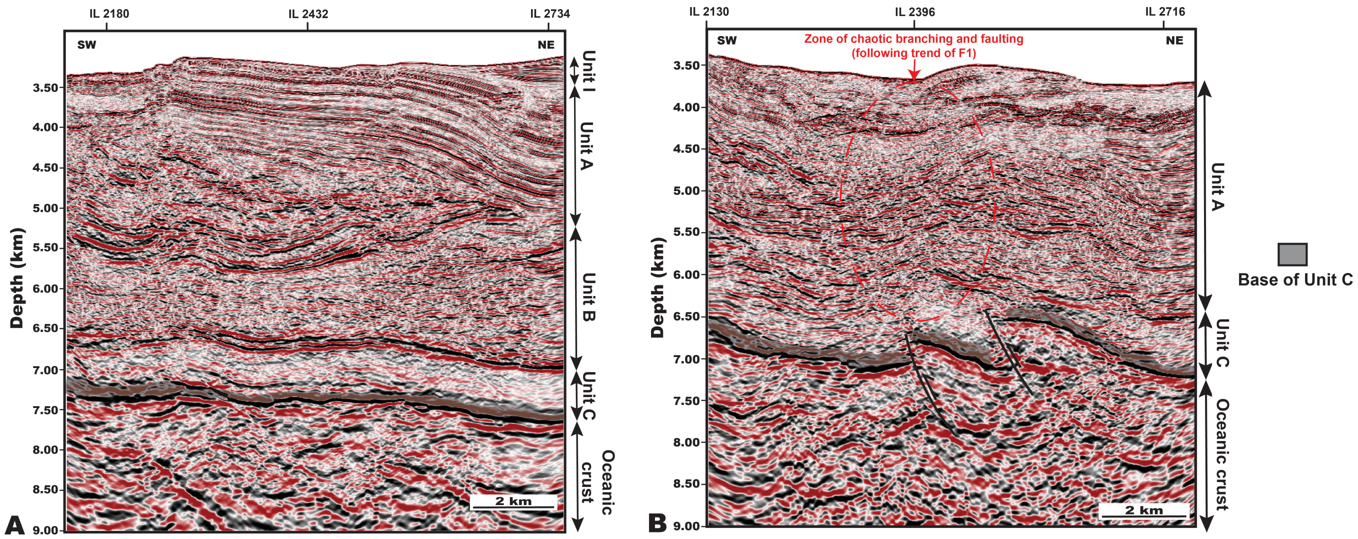

Fig. 7. Depth-migrated crossline 1571 (A) and 1139 (B) showing main tectono-stratigraphic units as described in Fig. 2 and the base of the subduction channel zone (SCZ). A) Unit C and underlying décollement present laterally continuous smooth bases, whereas the overlying Unit A deformed accordingly to the structure described in Fig. 4B. B) Here, both Unit B and the décollement below are folded and displaced by faults that follow the same trend as fault F1. Note the larger structural complexity in Unit A that results from the faults shown in B).

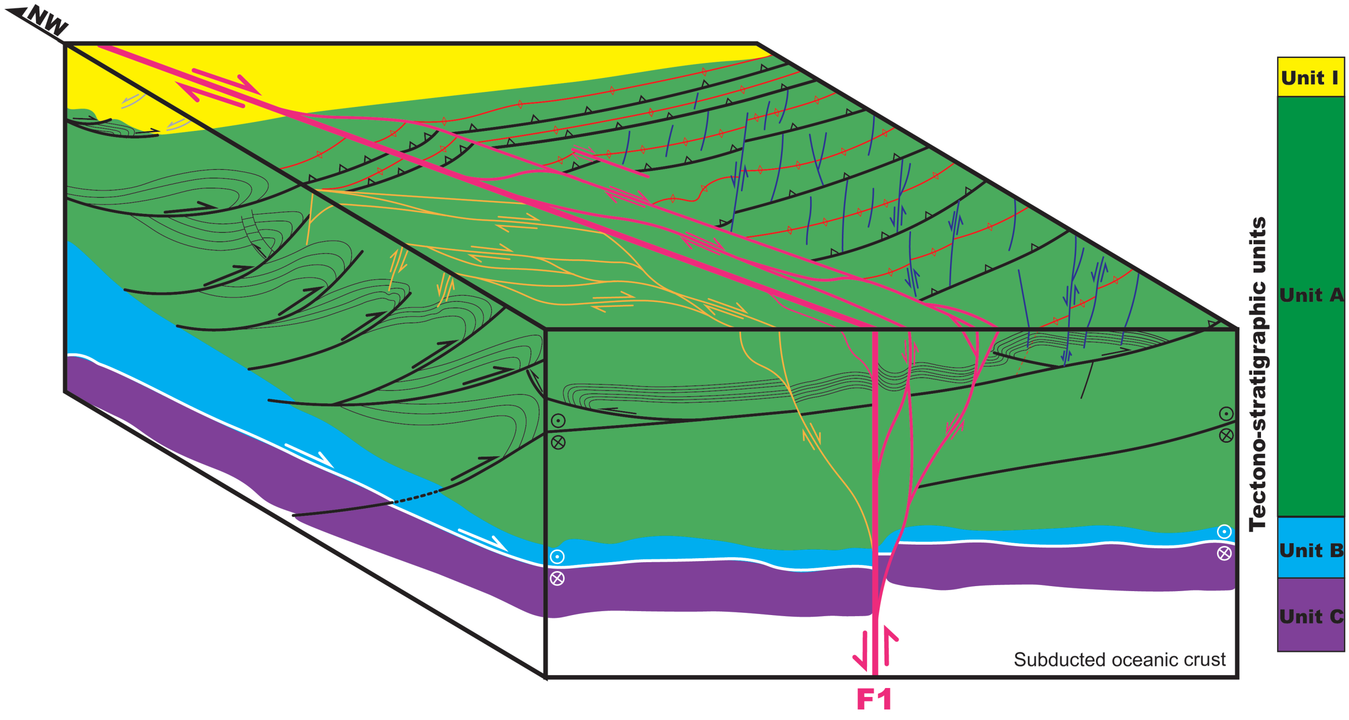

Fig. 8. Schematic block diagram summarising the structural framework of the outer wedge of the NAP (SE of the MSFZ and NW of the FTZ). The figure highlights the observed branching of fault F1 as reflecting a ‘flower structure’ separating two different structural domains. The NE domain is mainly characterized by well-developed thrust-and-fold structures with left- lateral strike-slip faulting occurring within the major anticlines. The SW domain is characterized by right-lateral strike-slip faults. The relative vertical displacement is not constant in the strike-slip faults within the NAP, meaning these latter are associated with important lateral motion. Red lines – axial planes of thrust anticlines; black lines – synthetic and antithetic thrust faults and corresponding anticlines; pink lines – WNW-trending right-lateral strike-slip faults; orange lines – E-W trending right-lateral faults; blue lines – NNW- to N-trending left-lateral strike-slip faults; grey lines – normal faults in Unit I; white line – décollement fault; half-arrows – relative movement of faults identified on seismic data; pair of circles - relative movement of faults identified on seismic data, where the circle with a dot indicates movement of block toward the reader, and the circle with the cross indicates movement away from the reader.

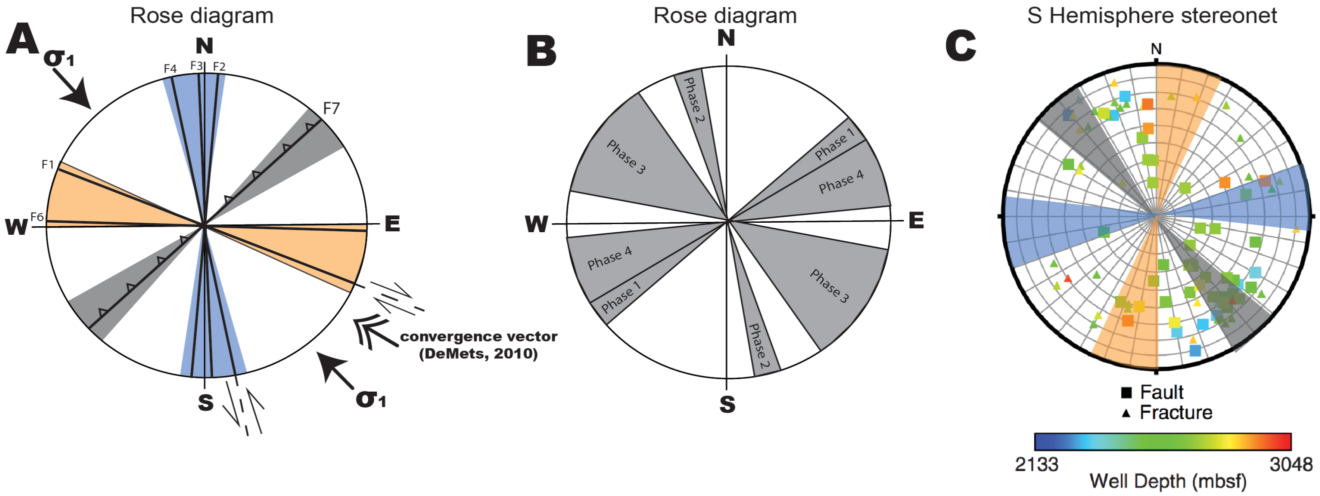

Fig. 9. A) Rose diagram highlighting the range in trends for fault families in the NAP. B) Rose diagram with the trends of each family of normal faults, and their chronological order, according to Moore et al. (2013). C) Lower-hemisphere Schmidt Stereonet with structural data from IODP Site C0002P as analysed in Boston et al. (2016) (note: trends in rose diagrams are rotated 90o from those shown in the stereonets).

left-lateral strike-slip faults. Orange – range of strikes of WNW- to E-W trending right-lateral strike-slip faults.